The Response of Waves to Changes in Wind Speed

Astrid M. van Agthoven

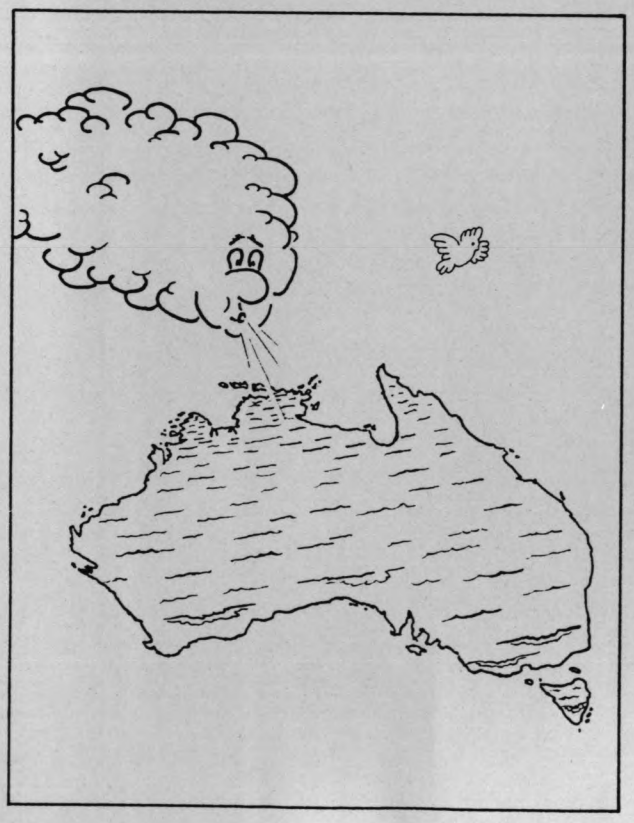

Delft University of Technology
Faculty of Civil Engineering
Division of Hydraulic and Geotechnical Engineering
Section Fluid Mechanics

The Response of Waves to Changes in Wind Speed

Astrid M. van Agthoven
May 1994

Supervision:
Prof.dr.ir. J.A. Battjes
Dr.ir. J. van de Graaff
Dr.ir. L.H. Holthuijsen
Dr. I.R. Young

Delft University of Technology
Faculty of Civil Engineering
Division of Hydraulic and Geotechnical Engineering
Section Fluid Mechanics

Preface

This report was written as a Master's thesis at the Faculty of Civil Engineering, Section Fluid Mechanics, of Delft University of Technology. Most of the work was done at the University of New South Wales in Canberra, Australia, where was cooperated in a wave measuring project at a lake.

The first part of this report deals with the response of the wave spectrum after a sudden change in wind speed on the basis of an academic numerical model. In the second part wave measurements during changing wind speed are analysed and compared with the results of the academic model and an operational model.

I thank everybody who had a contribution to this report, either with respect to content, personal or practical.

Delft, May 11th 1994
Astrid van Agthoven

Contents

Summary

Detailed studies have been carried out for fetch and duration limited wave growth and fully developed sea state, but much less is known about changing wind conditions. The subject of this study is the response of waves to a change in wind speed. The main point of interest is the rate of response at the different frequencies.

Two third generation wave prediction models were used, WAVEWATCH (Tolman, 1991) and the model of Resio and Perrie (1991). In third generation models all relevant processes of generation and dissipation of energy are represented explicitly by the three source terms: input of energy from the wind, nonlinear interactions between spectral components and dissipation of wave energy by various mechanisms. The main difference between the two used models is the way they calculate the nonlinear interactions. The operational model WAVEWATCH uses an approximation; the academic model of Resio and Perrie gives a full solution of the nonlinear source term. To reduce the computation time required to calculate all wave-wave interactions, this model is restricted to either duration or fetch limited wave growth in deep water.

With the model of Resio and Perrie a series of calculations was performed for sudden increases and decreases in wind speed. A simple equation which describes the model behaviour was formulated. An important coefficient of this equation is the adjustment rate immediately after the change in wind speed. Another meaningful parameter of the model behaviour is the time needed to reach a new equilibrium. Both parameters show that the rate of response increases with increasing frequency. The adjustment to a new equilibrium is faster for larger increases in wind speed, but slower for larger decreases.

Field measurements of wind speed, direction and wave height were carried out on Lake George near Canberra (Australia). Analysis of the wind data resulted in five cases with a clear change in wind speed and a sufficiently constant wind direction. These cases were analysed with Fast Fourier Transforms. The measurements were compared with the results of WAVEWATCH and the model of Resio and Perrie. The measurements were done in a water depth of about 2 meters; transitional water depth for the considered situations. Because in the model of Resio and Perrie bottom influence cannot be taken into account, the comparison with the measurements is only meaningful in situations with relatively short waves, which are not influenced by the limited depth of the lake. In these situations the results are reasonable. The results of WAVEWATCH do not agree very well with the measurements, e.g. the significant wave heights are too small. The parameterizations of the source terms need to be adjusted to the circumstances at the lake. The bottom roughness is probably much smaller than the 'standard' roughness for oceans.

1. Introduction

1.1 Scope

At the beginning of the nineteenth century Sir Francis Beaufort devised a numbering system for a descriptive wind scale, later extended to a scale of equivalent wind speed. This numbering system may be seen as the precursor of modern operational analysis and prediction of wind waves. Until World War II this was the only operational procedure for describing sea state. At that time there was a need for wave forecasts for the planning of the amphibious landing of troops in the Pacific region and France. For this reason Sverdrup and Munk made a serious study on wave analysis and prediction, which led to the first operational wave prediction procedure in 1943.

Because wave analysis and prediction techniques are very useful in coastal engineering, offshore technology and navigation, the development of wave prediction models continued. Some of the reasons why wave analysis started relatively recently are the difficulties and costs of reliable measurements and the mathematical difficulties involved. Because of the apparently chaotic character of wind waves, it is not possible to give a deterministic description of the sea state at every point and time. Instead of a deterministic description a probabilistic approach is necessary.

A convenient, often used way to describe wind waves is with the help of energy or variance spectra. In a linear approximation the wave field can be considered as the sum of an infinite number of independent sinusoidal waves. Each sinusoidal wave or wave component is characterised by a deterministic frequency, amplitude and direction and a random phase (random phase model).
The wave field can be presented as the squared amplitude as a function of frequency and direction. Because the squared amplitude of a component is proportional to its variance density and to the energy density this presentation of the wave field is called the variance or energy spectrum. If the two-dimensional (frequency and direction) energy spectrum is known, the statistical parameters of the occurring waves can be derived. Interesting parameters are for instance the significant wave height and period, mean wave height, mean direction and probability of exceedance of the wave height of a certain level.

In the spectral form the evolution of water waves can be described by the energy balance equation (for deep water without currents)

$$\frac{\partial E(f,\theta)}{\partial t} + c_g \cdot \nabla E(f,\theta) = S_{tot}(f,\theta) \qquad (1.1)$$

where $E(f,\theta)$ is the energy density, c_g the wave group velocity and S_{tot} the total source term.

Above equation forms the basis of recent wave prediction models (e.g. WAM Model, WAMDI Group 1988). The terms on the left hand side of the equation represent the accumulation of energy per unit of time and the propagation of energy at the wave group velocity c_g. The term on the

right hand side is the source term which represents the net amount of energy added to a wave component per unit of time.

The source term consists of three components

$$S_{tot} = S_{in} + S_{nl} + S_{ds} \tag{1.2}$$

where S_{in} represents the input of energy from the wind, S_{nl} the nonlinear interactions between spectral components and S_{ds} the dissipation of energy due to white capping and turbulence.

The many different wave models that have been developed, have been classified by the SWAMP study (Sea WAve Modelling Project, 1985) as first, second and third generation models. First generation wave models (1960s, early 1970s) do not include the nonlinear wave-wave interactions. Each spectral component evolves independently of other components. Although these models were applied for many years, they have two shortcomings:

- they underestimate the observed wave growth
- they are unable to explain the overshoot phenomenon of growing wind sea.

The overshoot effect is the phenomenon that developing waves do not always grow monotonically to their saturation level. They can grow beyond this level by a considerable amount and return to the saturation level afterwards. This phenomenon is considered to be an important factor in the wave generation process and is believed to be caused by the nonlinear interactions. To overcome these problems second generation models were developed. Because it was not possible to give a universal solution for the nonlinear source term at that time, these wave models use a parameterized version of the wave-wave interaction process. This simplified representation of the nonlinear source term requires restrictions on the spectral shape. This meant that the second generation models were unable to predict complex wind seas generated by rapidly changing wind.

Much progress has been made with the introduction of third generation models, the highest level of development presently reached. In third generation models all relevant processes of generation and dissipation of energy are represented explicitly. This means that for each of the three source terms of the energy balance equation quantitative expressions are used. Details about these expressions can be found in chapter 3.
Because the source terms can be calculated for every frequency and direction, the spectral energy of each wave component can be calculated for arbitrary wave fields with these models.
Although the physical processes are not fully clear and consequently the expressions for the source terms are still approximations, the third generation wave models are adequate operational wave prediction models.

1.2 Problem description

It is generally known that it takes a finite time for the wave spectrum to adjust to a changing wind speed. Low frequency waves respond slowly to a change in wind speed. The adjustment of high frequency waves, on the other hand, is so fast that it can be considered as an instantaneous response.

Satellite based microwave instruments such as the scatterometer can image the high frequency portions of the wave spectrum. Assuming that this section of the spectrum is in equilibrium with the wind, enables to make an estimate of the wind speed. However, the rate of adjustment of the different frequencies to a change in wind speed is unknown.

Detailed studies have been carried out for fetch and duration limited wave growth and fully developed sea state (e.g. Hasselmann et al., 1973; Donelan et al., 1992). Much less is known about changing wind conditions. A few studies have been made of changing wind direction (e.g. Hasselmann et al., 1980; Günther et al., 1981; Holthuijsen et al., 1987; Young et al., 1987; Van Vledder & Holthuijsen, 1993), but to the author's knowledge only one study has been carried out for changes in wind speed (Toba et al., 1988).

In order to increase the practical knowledge and the understanding of the physical processes involved, the response of waves to changes in wind speed has been analysed in this study. This has been done by a numerical experiment with the one dimensional third generation numerical model of Resio and Perrie (1991) which takes all nonlinear interactions into account, and by field measurements on Lake George (see figure 1.1) hindcasted with the above mentioned model and the third generation model WAVEWATCH (Tolman, 1991).

Figure 1.1 Lake George

1.3 Approach

In chapter 2 the results of a literature review of waves in transient conditions can be found.
The main features of the two used numerical models are described in chapter 3.
The numerical experiment involves a series of calculations with the model of Resio and Perrie for a number of ideal changes in wind speed. The results are analysed to obtain insight in the behaviour of the model. This is presented in chapter 4.
Chapter 5 describes the way the field measurements were carried out and the processing of the measurements to workable data.
The most suitable measured data has been simulated with both numerical models. Similarities and discrepancies are discussed in chapter 6.
Conclusions of this study are presented in chapter 7.

2. Previous Studies of Transient Wind Conditions

2.1 The response of waves to changing wind direction

The directional response of wind waves has been the subject of several studies, e.g. Hasselmann et al. (1980) among the first. Analysing the measurements of two buoys in veering wind situations they found good agreement between the rate of change of the wave direction and the wind direction for high frequencies, while the directions at the lower frequencies adjust more slowly to a new wind direction. Very low frequencies keep the old direction and are considered as swell.

As a simple model to describe the observations they proposed

$$\frac{\partial \theta_{0,f}}{\partial t} = \omega b \sin(\theta_w - \theta_{0,f}) \tag{2.1}$$

in which $\theta_{0,f}$ is the mean wave direction as a function of frequency, θ_w is the wind direction, ω the radian frequency and $b=b(U/c;f/f_p)$ a relaxation coefficient with f_p the peak frequency, U the wind speed and c the phase velocity. They found $b \approx 2.10^{-5}$.

This relaxation model was used in many other studies on this subject in slightly different forms. The factor ωb is usually replaced by τ^{-1}, where τ is called the time scale. The model assumes that the rate of change of the wave direction, θ_0, is determined by the angle between the wind direction θ_w and the wave direction θ_0. According to Quanduo and Komen (1993) it is better to use the angle between the mean direction of the rate of change of the spectrum, $\theta_{\partial E/\partial t}$, and θ_0. However, because it is difficult to measure $\theta_{\partial E/\partial t}$, this direction is usually approximated by θ_w.

Allender et al. (1983) also determined the relaxation coefficient b of equation (2.1) from observations . They found values of b within the same ranges of Hasselmann et al. (1980).
In the studies of Allender et al. (1983) and Hasselmann et al. (1980) the relaxation is described for single frequencies, which results in frequency dependent time scales τ. Instead of a frequency dependent time scale Günther et al. (1981) averaged the directional behaviour over the frequencies resulting in the following model

$$\frac{\partial \theta_0}{\partial t} = \chi \frac{f^2}{g} U \sin(\theta_w - \theta_0) \tag{2.2}$$

with θ_0 the mean direction of the spectrum. Using the same data as Hasselmann et al. (1980) they found $\chi \approx 0.21.10^{-2}$.

Holthuijsen et al. (1987) quantified the time scale τ of relaxation models by using universal growth characteristics of waves in an ideal situation in which a homogeneous wind field starts

blowing over an infinite ocean at t = 0. From the premise that the net wave growth is centred around the wind direction they derived that the relaxation model can also be written as

$$\frac{\partial \theta_0}{\partial t} = \frac{1}{\epsilon}\left(\frac{\partial \epsilon}{\partial t}\right)\sin(\theta_w - \theta_0) \tag{2.3}$$

in which ϵ is the total wave energy

$$\epsilon = \int_0^\infty E(f)df \tag{2.4}$$

In dimensionless form equation (2.3) gives

$$\frac{\partial \theta_0}{\partial \tilde{t}} = \frac{1}{\tilde{\epsilon}}\frac{\partial \tilde{\epsilon}}{\partial \tilde{t}}\sin(\theta_w - \theta_0) \tag{2.5}$$

in which $\tilde{t} = gt/U$ and $\tilde{\epsilon} = \epsilon g^2/U^4$, where U is the wind speed.

The evolution of ϵ can be approximated with $\tilde{\epsilon} = a \tanh^d(b\tilde{t}^c)$ (SWAMP study 1985). The values of the coefficients a,b,c, and d were chosen as more or less an average of all SWAMP growth curves. Holthuijsen et al. (1987) determined τ with help of observed growth rate of the wave energy, the above mentioned growth curve and pitch-and-roll buoy observations. The time scale determined by the observations and the universal growth curve are consistent with the results of Günther et al. (1981). The theoretically expected dependency of τ on the dimensionless energy could not be confirmed by the observations.

Young et al. (1987) compared the results of two numerical models with each other and with field observations of Hasselmann et al. (1980) and Allender et al. (1983). Both models give quite similar results. The models show that for wind shifts of 30° and 60° the entire spectrum rotates to the new wind direction. The high frequencies respond almost instantaneous as immediately after the wind shift the total source term balances at these frequencies.
The input of energy from the wind shows two peaks, one in the old wind direction and a higher frequency peak in the new wind direction. The new peak is counteracted by the nonlinear interactions because the nonlinear interactions develop a negative contribution to the total source term in the area of the new peak.
A wind shift of 90° or more gives a second peak that initially develops a little beside the new wind direction, biased to the old wind direction. This is caused by the fact that the energy input by the wind needs some initial level of energy to become effective. The new peak quickly adjusts to the wind direction, grows and moves to lower frequencies. The old sea gradually decays by dissipation. In these cases the two seas are so far from each other in directional space that there is

no nonlinear coupling between them.
At comparable values of U/c the time scale of the models agrees with the data of Hasselmann et al. (1980) and Allender et al. (1983).

Van Vledder and Holthuijsen (1993) did a numerical experiment too and compared it with directional wave observations. The observed time scales are generally two to three times shorter than the model results. In the numerical model for both small and large wind shifts a second peak developed, rapidly merging with the old peak for small shifts. These numerical calculations were for more developed sea states than those of Young et al. (1987). As the time scales for younger sea states are smaller than for relatively older waves the response of the waves in the cases of Young et al. (1987) were so fast that a second peak was not visible for the small wind shifts.
The behaviour of the source terms of the model is as follows. The atmospheric input generates energy at the high frequencies between the old and new wind direction. For a small wind shift this process still supports the old spectrum. The nonlinear interactions have a positive contribution to the net source term for the old direction and negative for the new direction. The dissipation of energy is largest in the new direction. So both the nonlinear interactions and the dissipation counteract the turning of the wave direction. Whitecapping appears to be a stronger process than the effect of the nonlinear interactions.
It is speculated that at some moment during a turning wind event the role of the nonlinear interactions changes from opposing to supporting the turning of the waves. This is based on the property of the nonlinear interactions to support a unimodal spectrum. The nonlinear interactions would support the prevailing peak, shifting from the old to the new peak.

2.2 The response of waves to changing wind speed

Only one paper about the response of wind waves to changing wind speed was found (Toba et al., 1988). The most important features are summarised below.

Phillips (1958) proposed on dimensional grounds a form of the one-dimensional frequency spectral density E(ω) of wind waves for the high frequency side of the spectral peak (= equilibrium range)

$$E(\omega) = \beta g^2 \omega^{-5} \tag{2.6}$$

where ß is a dimensionless constant.
Based on empirical data and with the aid of dimensional analysis, Toba (1973) proposed another form for the equilibrium range

$$E(\omega) = \alpha_s g_* u_* \omega^{-4} \quad , \quad g_* = g\left[1+\frac{Sk^2}{\rho_w g}\right] \tag{2.7}$$

with α_s a constant, u_* the air friction velocity at the water surface, S the surface tension, k the

wave number and ρ_w the density of water. This spectral form has also been found in other experiments, although there is a difference in observed values of α_s which ranged between 6 x 10^{-2} and 11 x 10^{-2} (Phillips, 1985). The physical interpretation of equation 2.7 is sought in overall constraints imposed by the coupled turbulent boundary layers of air and water. This implies that the processes responsible for the adjustment of wind waves to a change in wind are strongly nonlinear.

Three series of observations are analysed in the paper. In these observed situations the wind fluctuates with a general trend to increase. If the energy level of the equilibrium range of frequencies immediately follows the change of u_*, α_s would be a constant. The observations show that α_s becomes smaller for increasing wind and larger for decreasing wind on short time scales, but the general trend of α_s is to remain constant. This means that the energy level does not follow the change in u_* immediately, but it adjusts itself to the variation of the wind on a larger time scale. This timescale is in the order of several minutes, which is faster than the time scale of the growth of the total energy of the spectrum. So the high frequency tail responds faster than the low frequencies.

When the wind increases rapidly, the peak frequency shifts to higher frequencies presumably caused by an increase of energy supply of the nonlinear interactions at the high frequencies at the expense of energy near the spectral peak. When the equilibrium at the high frequencies is restored, the growing total energy forces the peak frequency to lower frequencies. For decreasing wind speed the opposite happens.

The peak of the spectra is broad when u_* is increasing and narrow for decreasing u_*. This indicates that for increasing wind speed the energy of the waves on both sides of the spectral peak are fed. When u_* is decreasing the energy on both sides of the peak decreases, feeding the waves at the peak frequency. In this way the spectral peak remains symmetrical.

3. Numerical Models

3.1 Introduction

In this chapter the solution of the energy balance equation, especially the three source terms, is treated in general and with respect to the two numerical, third generation models used in this study. The numerical models that have been used are the model of Resio and Perrie (1991) and WAVEWATCH, the model of Tolman (1991).

The model of Resio and Perrie (referred to as Resio's model in the following) is a third generation wave model with a full solution of the nonlinear interactions. Because of the enormous computation time WAVEWATCH uses an approximation for the nonlinear source term, like most wave models.

Calculation of all nonlinear interactions within acceptable computation time causes some restrictions of the model in other respects.
The differential equation (1.1) has to be simplified to one dimension, either duration limited growth

$$\frac{\partial E(f,\theta)}{\partial t} = S_{tot}(f,\theta) \tag{3.1}$$

or fetch limited growth,

$$c_g \cdot \nabla E(f,\theta) = S_{tot}(f,\theta) \tag{3.2}$$

The version for duration limited growth, used in this study, assumes $\nabla E=0$, so no spatial variation, i.e. an ocean with infinite dimensions.

A second limitation is that bottom influence can not be incorporated without very large increase of the computation time, because only in deep water the nonlinear interactions show some regular features that make it possible to simplify the calculations.

For the numerical experiment of chapter 4 Resio's model was used, since it gives the best representation of the physics behind wave generation because of the full solution of the nonlinear interactions. A second reason for the choice of this model is the fact that the model is relatively simple because of the above mentioned restrictions. This allows insight in the model behaviour, which is a requirement for a numerical experiment.

WAVEWATCH is an operational, third generation wave model, which does not have these restrictions of infinite depth and fetch. This makes it more suitable to hindcast the measured data

of Lake George. Both WAVEWATCH and Resio's model were used to compare the measurements with numerical calculations.

In WAVEWATCH equation (1.1) is solved by treating the propagation and source term integration separately. Various schemes are available. Here a first order upstream scheme is used for the propagation, which is calculated before the source term integration. The source term is integrated with a straightforward explicit (Euler) integration. This is the same integration scheme as used in Resio's model to solve equation (3.1).

3.2 Wind input

The transfer of energy and momentum from the wind to waves is an intricate, turbulent process at the transition between air and water. In this process two phases can be distinguished.
In the first phase the wind profile is not influenced by the waves. Phillips (1957) found that in this phase the energy density of a wave component increases linearly with time.
In the second phase, analysed by Miles (1957), the wind profile is affected by the waves. In this phase the rate of input of energy to a wave component is proportional to the energy density of that wave component, so the energy density grows exponentially with time.

The input source term of the energy balance can be modelled as the summation of linear and exponential growth

$$S_{in}(f,\theta) = A + BE(f,\theta) \tag{3.3}$$

in which A and B are functionals of the energy density E(f,θ) and the wind vector.
Because the exponential growth term is much larger than the linear term, the linear term is often omitted in wave prediction models.

The equation for wind input used in both models is the formulation of the source term by Snyder et al. (1981), scaled to the friction velocity u_* by Komen et al. (1984) instead of the wind speed U_5 at 5 meters height

$$S_{in}(f,\theta) = \max\{\ 0\ ,\ 0.25\frac{\rho_a}{\rho_w}\omega(28\beta(\frac{u_*}{c})\cos(\theta-\theta_w)-1)E(f,\theta)\} \tag{3.4}$$

where ρ_a is the density of air, ρ_w is the density of water, ω is the radian frequency, c is the phase velocity, θ is the direction of the spectral component, θ_w is the wind direction and β is an empirical coefficient close to unity. This formula implies that $S_{in}=0$ if the angle between the direction of the wave component and the wind direction is larger than 90° or u_* is small compared to the phase velocity.

3.3 Dissipation of wave energy

Two main mechanisms of wave energy dissipation can be distinguished, wave breaking (in deep water referred to as whitecapping) and energy dissipation due to wave bottom interactions. Both mechanisms are still poorly understood.

Wave breaking is a very complicated, strongly nonlinear process. In both models the expression for wave breaking proposed by Komen et al. (1984) is used

$$S_{ds}(f,\theta) = -C\bar{\omega}\left[\frac{\omega}{\bar{\omega}}\right]^2\left[\frac{\hat{\alpha}}{\hat{\alpha}_{PM}}\right]^2 E(f,\theta) \tag{3.5}$$

with

$$\hat{\alpha} = \frac{E_{tot}\bar{\omega}^4}{g^2} \tag{3.6}$$

in which C is a constant, $\bar{\omega}$ the mean radian frequency, $\hat{\alpha}$ the integral mean wave steepness, and $\hat{\alpha}_{PM}$ the theoretical value of $\hat{\alpha}$ for a Pierson-Moskowitz spectrum. This equation is based on general assumptions for any nonlinear, small-scale and local process (Hasselmann, 1974).

Dissipation of wave energy due to wave-bottom interactions can be caused by three mechanisms, i.e. percolation, bottom motion and bottom friction. Percolation takes place in very porous soils, bottom motion in cases of soft mud and vegetation. The most important mechanism is bottom friction, because it is the main process for sand bottoms as found in many seas.
Wave-bottom interactions are not taken into account in Resio's model. In WAVEWATCH the parameterization for bottom friction of Madsen et al.(1988) was used, which can be written as

$$S_{bot}(f,\theta) = -\frac{8}{3\pi}f_w u_{b,r}\frac{k}{\sinh 2kd}E(f,\theta) \tag{3.7}$$

where f_w is a non-dimensional friction factor, d the water depth and $u_{b,r}$ is a representative near-bottom orbital velocity.

3.4 Nonlinear wave-wave interactions

In addition to the atmospheric input and the dissipation term there is a third, less obvious, though important source term caused by the nonlinear wave-wave interactions, first introduced by Hasselmann (1960) and Phillips (1960). The principle of wave-wave interactions is that a group of wave components in a special configuration can supply energy to another wave component.

Hence, the wave components do influence each other by exchanging energy. In many applications the wave field is considered as the sum of a large number of independent wave components, a linear system. For small time and space scale the energy exchange is so small that it can be neglected. For computations over long periods and large areas the nonlinear effects are considerable. Measurements (JONSWAP, Hasselmann et al. 1973) suggest that the nonlinear interactions play an important role in the evolution of the energy spectrum.

The nonlinear wave-wave interactions have a few characteristic features. The interactions do not supply to, or remove energy or momentum from, the wave field; they only redistribute momentum and energy among spectral components. An important property of nonlinear interactions is that the peak of the spectrum gains energy at the expense of higher frequencies for broad spectra (Hasselmann, 1963 and Webb, 1978) and the peak of narrow spectra tends to lose energy especially to frequencies below the spectral peak (Hasselmann et al., 1973). This results in a shift of the peak frequency towards lower frequencies.
Another effect of the nonlinear interactions is that they stabilise the shape of the spectrum. Small, local perturbations of the spectrum are smoothed out as a result of the redistribution of wave energy by nonlinear interactions (Young and Van Vledder, 1993).

Hasselmann (1962) developed a theory for the nonlinear interactions. He found that a set of 4 waves, a quadruplet, can exchange energy, if it satisfies the following two resonance conditions

$$\underline{k}_1+\underline{k}_2 = \underline{k}_3+\underline{k}_4 \tag{3.8}$$

$$f_1+f_2 = f_3+f_4 \tag{3.9}$$

The first condition conserves momentum, the second takes energy conservation into account.
He gave a formula for the nonlinear interactions in terms of action density n, the ratio of the energy E to the radian frequency. The rate of change in action density of a wave component due to all interactions involving this component, is given by the Boltzmann integral

$$\frac{\partial n_1}{\partial t} = \int\int\int G(\underline{k}_1,\underline{k}_2,\underline{k}_3,\underline{k}_4) \times \delta(\underline{k}_1+\underline{k}_2-\underline{k}_3-\underline{k}_4) \times \delta(\omega_1+\omega_2-\omega_3-\omega_4) \times [n_1 n_3 (n_4-n_2)+n_2 n_4 (n_3-n_1)]\, d\underline{k}_1 d\underline{k}_2 d\underline{k}_3 \tag{3.10}$$

where $\delta(...)$ the Dirac delta function and G the coupling coefficient

$$G = \frac{\pi g^2 D^2}{4\rho_w{}^2 \omega_1 \omega_2 \omega_3 \omega_4} \tag{3.11}$$

in which the interaction coefficient D is a complicated function of the four wave numbers.

The Boltzmann integral also conserves the wave action, because of the symmetry of the two pairs of wavenumbers ((k_1,k_2) and (k_3,k_4)) within one quadruplet. The absolute value of the rate of change of the action density is equal for all wavenumbers within the quadruplet

$$\frac{dn_1}{dt} = \frac{dn_2}{dt} = -\frac{dn_3}{dt} = -\frac{dn_4}{dt} \tag{3.12}$$

This is useful in methods for the computation of the nonlinear transfer.

Numerical integration of the Boltzmann integral is very time consuming due to the six dimensions of the integral and to the complexity of the coupling coefficient G. Because of the excessive computer time full numerical solutions are impractical. An alternative for use in operational models is a parametric method. In parametric models the energy spectrum is approximated by a spectrum with a standard shape for which the nonlinear interactions were calculated previously with a full numerical solution technique.

An obstacle for the calculation and understanding of the nonlinear interactions is the difficulty to visualise the interaction space. Webb (1978) introduced a visualisation technique for the interaction space for fixed k_1 and k_3. In this case the possible values of k_2 and k_4, which satisfy the conditions (3.8) and (3.9) form two 'egg-shaped' figures, called loci. See figure 3.1 (after Young and Van Vledder 1993). The solution of the integral can now be reduced to the evaluation of a series of line integrals around the loci. Although this simplifies the problem, the number of possible loci is enormous. Hence, the computation time is still too long to be used in wave prediction models.

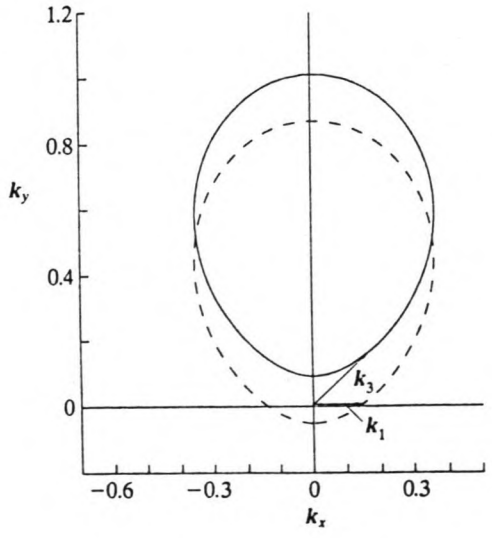

Figure 3.1 Loci of the vectors k_2 (——) and k_4 (---) for a given combination of k_1 and k_3

Tracy and Resio (1982) found that for deep water conditions the loci are geometrically similar. This permits the calculation of the k_2 and k_4 loci and the line integrals around the loci with a scaling technique. This is the method used in Resio's model.

Hasselmann and Hasselmann (1981) introduced a computation method, referred to as the symmetric method. This method uses the symmetry properties of both the Boltzmann integral and the interaction coefficient. This method, incorporated in the numerical wave prediction model EXACT-NL, calculates the interactions of about 600 000 quadruplets.
A simplified integration technique known as the discrete interaction approximation (Hasselmann et al., 1985) was developed on the basis of the symmetric method. Only one type of wave number configuration and its mirror image is used, reducing the number of quadruplets considerably. This method can give sufficiently accurate computations, because only a small amount of the huge number of quadruplets represents the largest part of the energy transfer. For the other interactions the energy transfer is very small.
The discrete interaction approximation made it possible to develop third generation global models. The method has been used in the WAM model (WAMDI group, 1988) and in WAVEWATCH.

4. Numerical Analysis of Sudden Change in Wind Speed

4.1 Runs performed

With Resio's model a series of runs was performed for the ideal situation that the wind speed suddenly increases or decreases. To simulate this, the program was run first with a constant wind speed for a while. Then a restart from the final situation of this run was made with a different wind speed. The moment of the restart is referred to as t = 0.
For both increasing and decreasing wind speed the program was run for an absolute change in wind speed of 5, 10 and 15 m/s during period of 4200 s.
In the case of increasing wind speed the program started from a situation with an initial wind speed U_0 of 10 m/s, in the case of decreasing wind speed U_0 was 20 m/s.
All runs were performed a second time starting with a more developed spectrum with a lower peak frequency. This peak frequency is referred to as f_{p2}, while the peak frequency of the initial spectrum of the runs described above is referred to as f_{p1}.

An overview of the runs performed is given in table 4.1. In this table all runs have been numbered to make it easier to refer to the runs in the following paragraphs.

		ΔU = 5 m/s	ΔU = 10 m/s	ΔU = 15 m/s
increasing wind	f_{p1} = 0.24 Hz	1	2	3
U_0 = 10 m/s	f_{p2} = 0.19 Hz	4	5	6
decreasing wind	f_{p1} = 0.19 Hz	7	8	9
U_0 = 20 m/s	f_{p2} = 0.14 Hz	10	11	12

Table 4.1 Runs performed

The program was run with a timestep of 5 s and a spectral resolution of $\Delta\theta$=6.67° and 43 frequencies, unevenly spaced according to $f_{i+1}=1.063f_i$ ranging from 0.0705 Hz to 0.9175 Hz.

4.2 Behaviour of the model

In this paragraph the behaviour of the model is shown on basis of the results of run 2 and 8. The other runs show the same trends, so they are not treated separately.

The figures 4.1 and 4.2 show the growth of the one dimensional spectrum for run 2 on a linear and logarithmic scale respectively. These figures show that first the most obvious growth occurs at frequencies higher than the peak frequency. Soon the highest frequencies do not gain energy any more. At the end the situation typical for growing wind sea has been reached. In that stage the peak of the spectrum is growing and moving to lower frequencies.

This behaviour can be understood by looking at the source terms at a few different times, see figure 4.3 a and b.
At t = 0 s the source terms show their characteristic features in a situation of growing wind sea. The input and dissipation terms are large around the peak frequency, gradually decreasing towards the high frequencies. The nonlinear term has a positive lobe just left and a negative lobe right of the peak frequency, staying negative for the high frequencies. This results in a total source term that balances for the high frequencies and a positive-negative lobe around the spectral peak. After the increase in wind speed the input term increases significantly, as expected. Hence the total source term becomes positive for all frequencies. The nonlinear interactions respond to the increasing wind speed by larger negative values at the highest frequencies and an extra positive lobe right of the spectral peak. In this way the nonlinear interactions force the total source term back to zero for the high frequencies and give energy to lower frequencies. Gradually the extra positive lobe disappears and all terms are back to a shape equal to the beginning.

For run 8, where the wind speed decreases from 20 m/s to 10 m/s, the energy spectra are shown in figure 4.4 on a linear scale and in figure 4.5 on a logarithmic scale. The changes in the spectra are smaller than in the case of an increasing wind speed. Again the high frequencies respond first. The source terms, see figure 4.6 a and b, show that only the input term drops significantly immediately after the change in wind speed, while the dissipation and nonlinear term are of the same order of magnitude as at t = 0 s. The total source term is negative everywhere except for a small peak due to the positive lobe of the nonlinear interactions.
All source terms gradually decrease in magnitude. At t = 4200 s the source terms are not back to their normal proportions yet, as in the increasing wind case. This indicates a difference in rate of the relaxation process for decreasing wind and the forced growth for increasing wind speed.

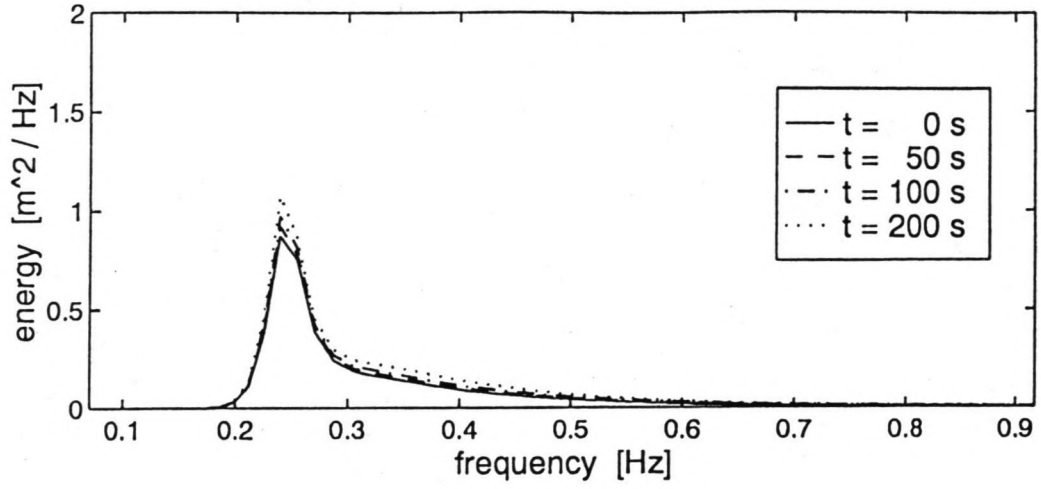

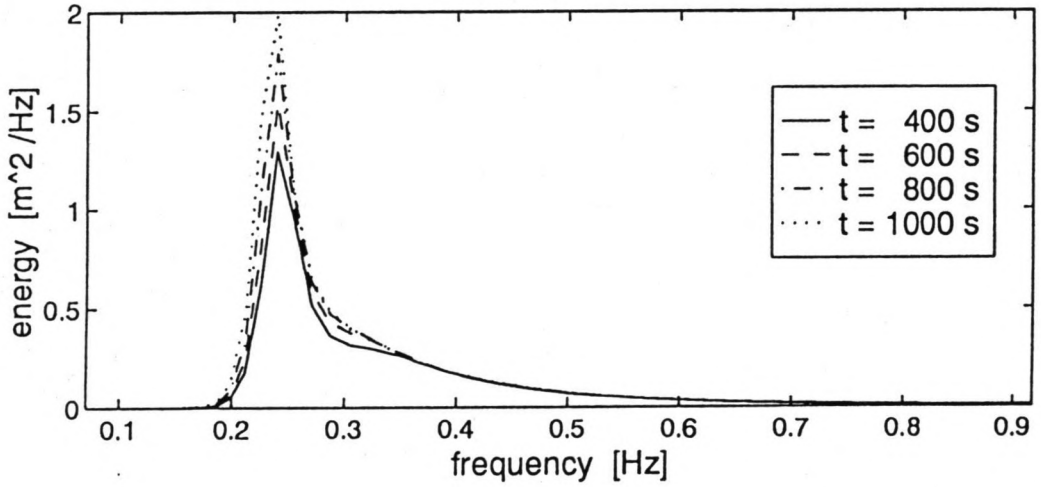

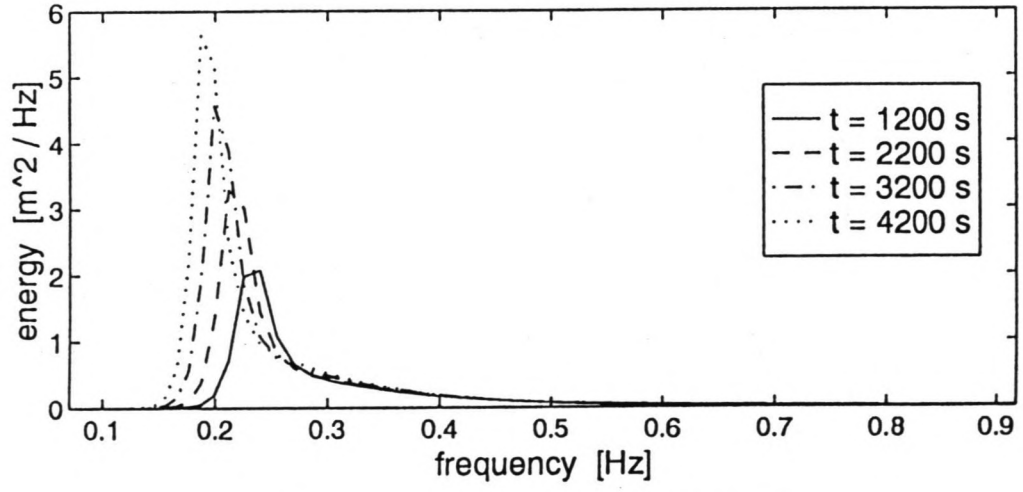

Figure 4.1 Spectra run 2 on linear scale

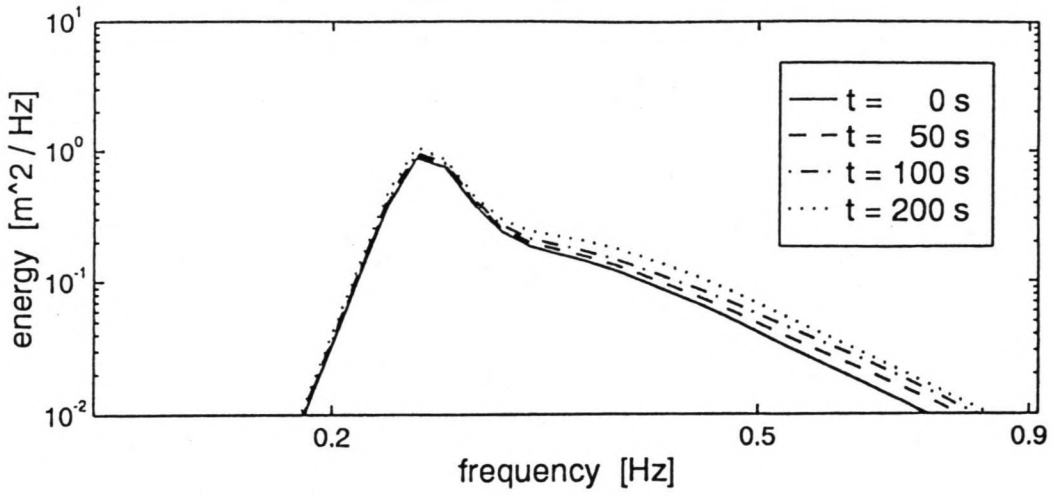

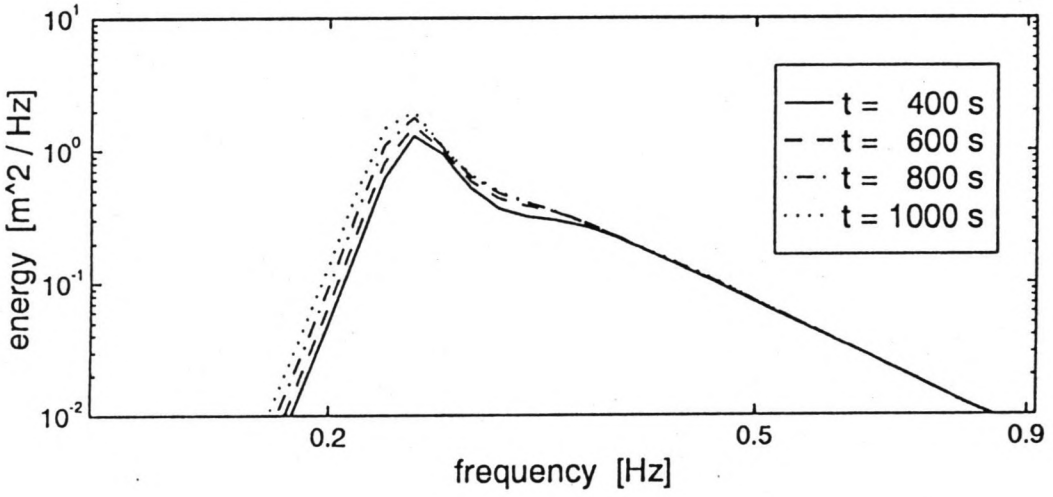

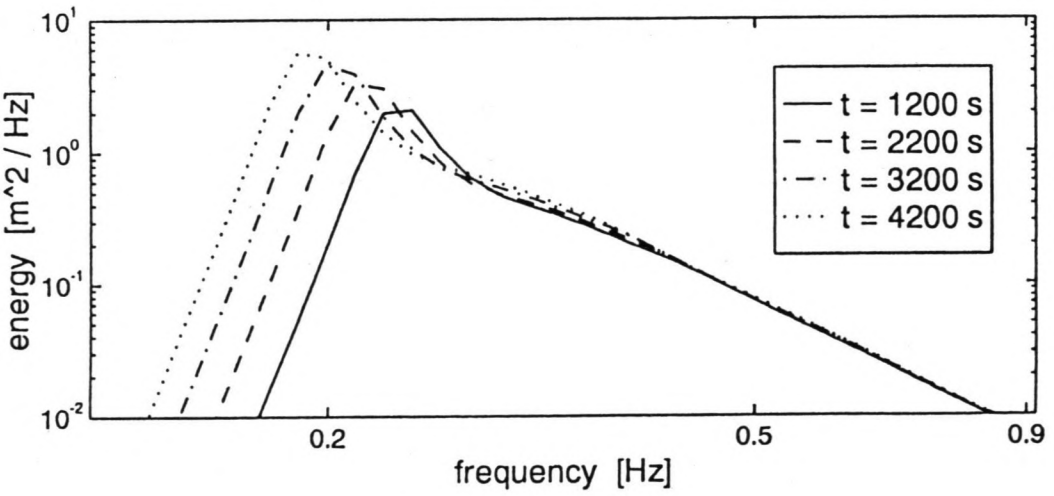

Figure 4.2 Spectra run 2 on logarithmic scale

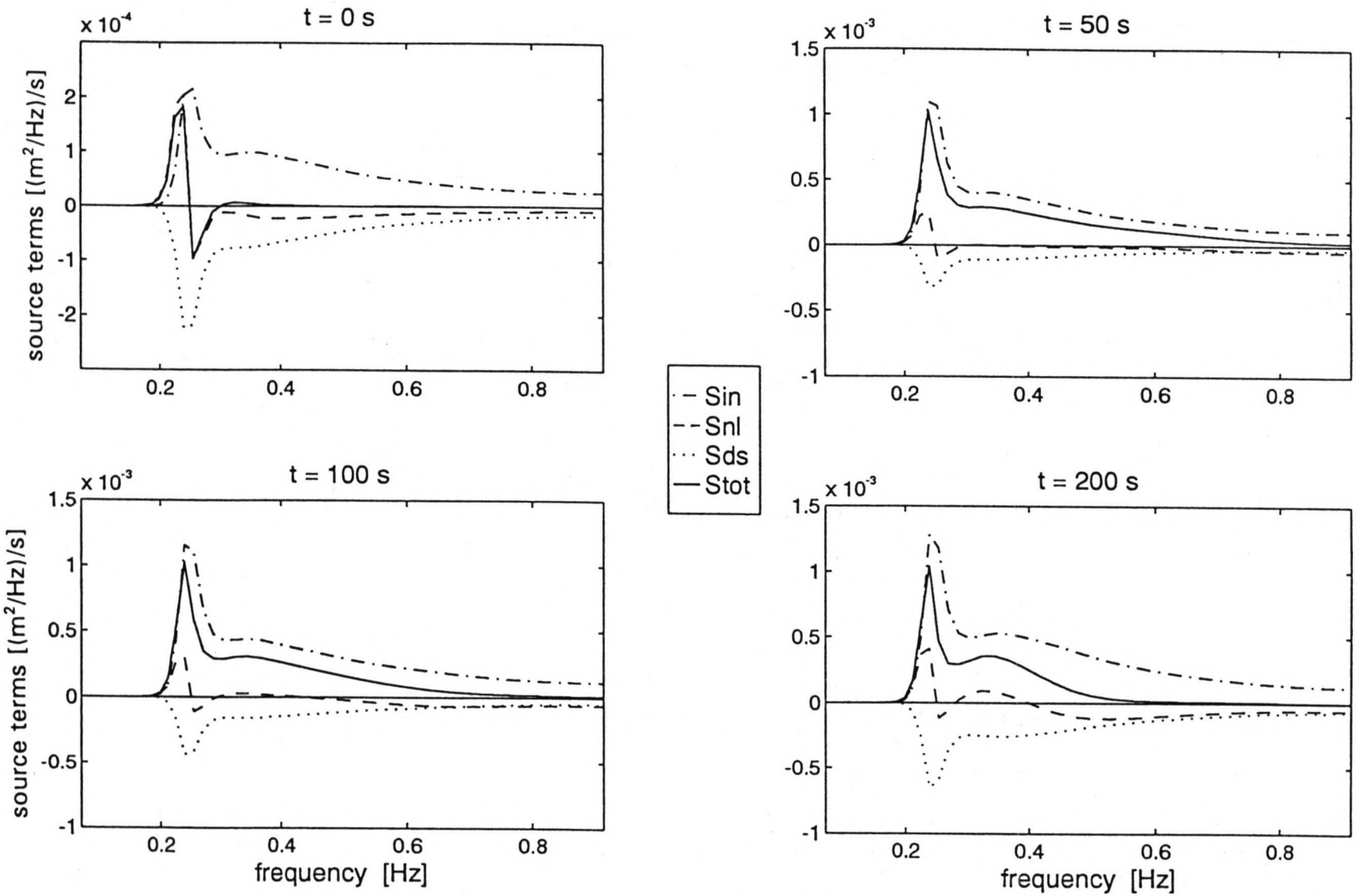

Figure 4.3 a Source terms run 2 (t = 0, 50, 100, 200 s)

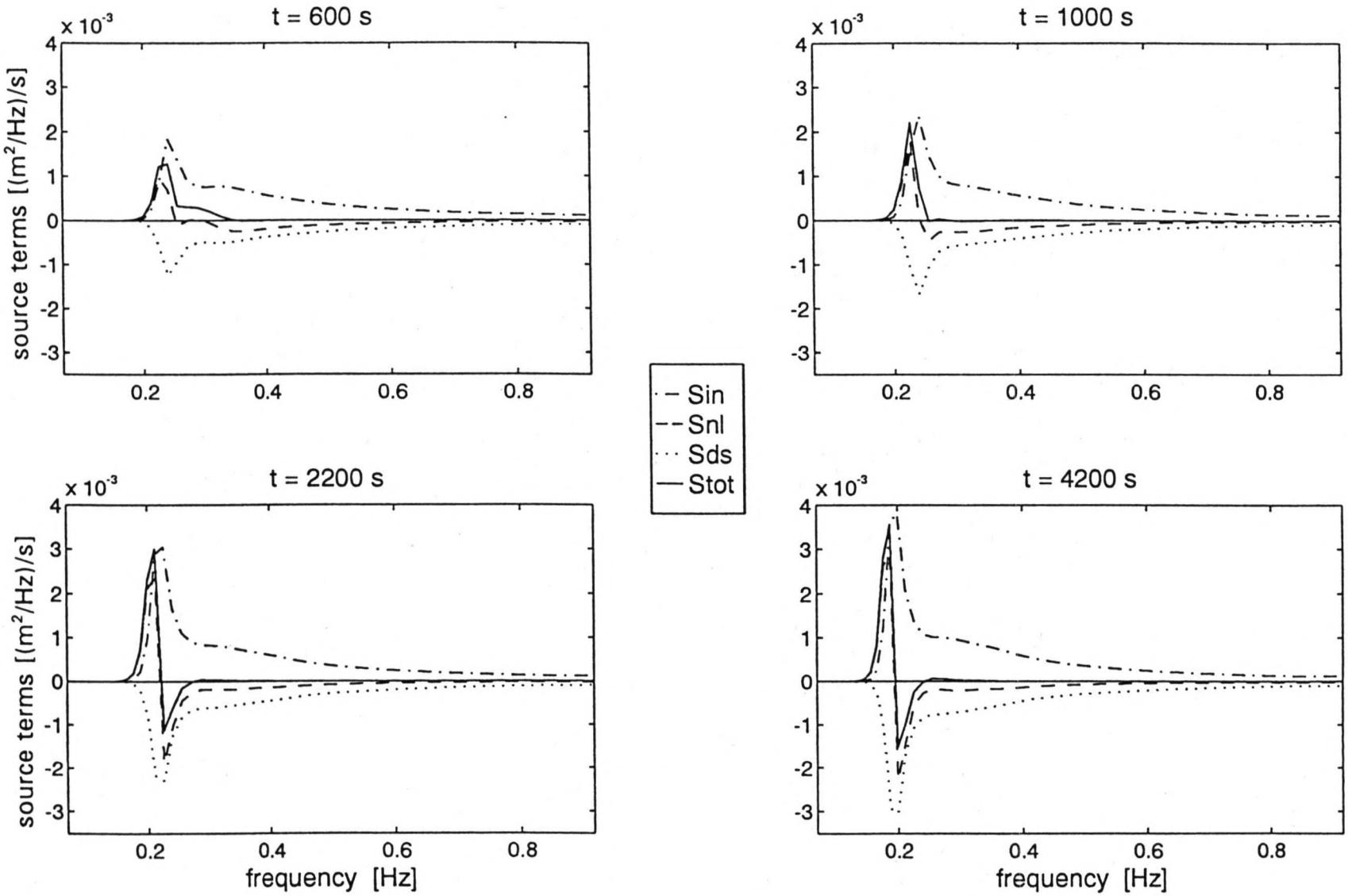

Figure 4.3 b Source terms run 2 (t = 600, 1000, 2200, 4200 s)

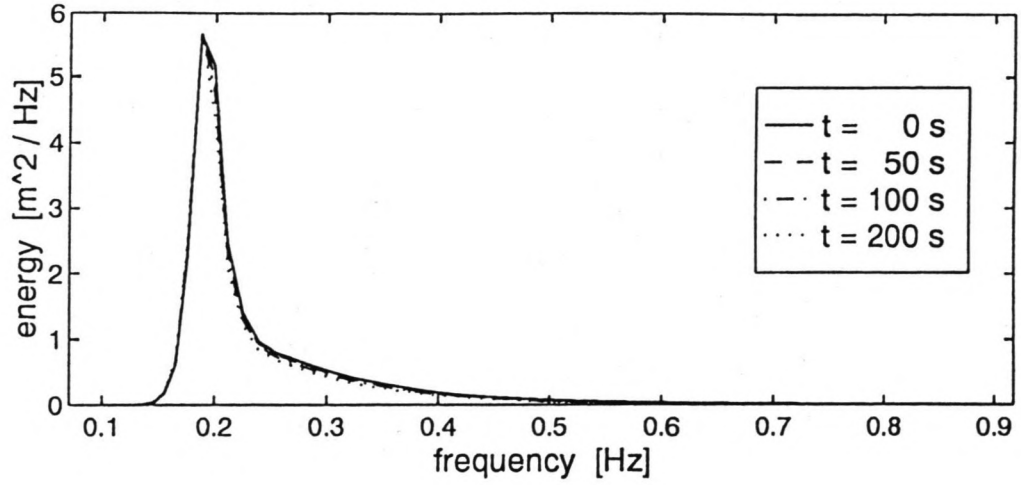

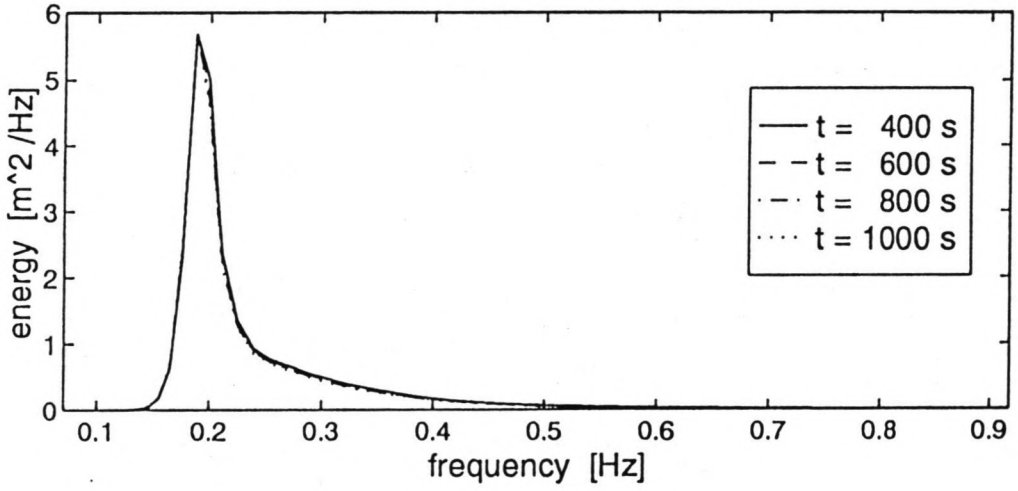

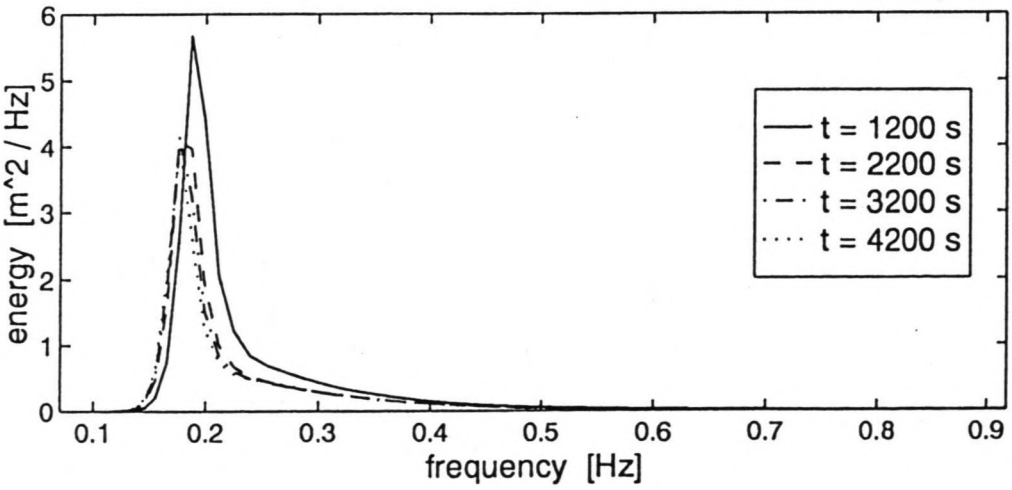

Figure 4.4 Spectra run 8 on linear scale

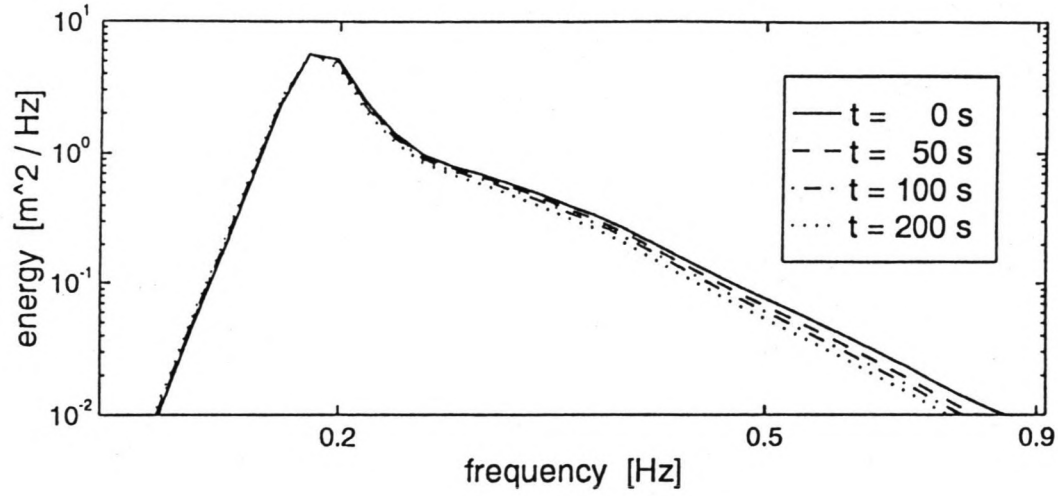

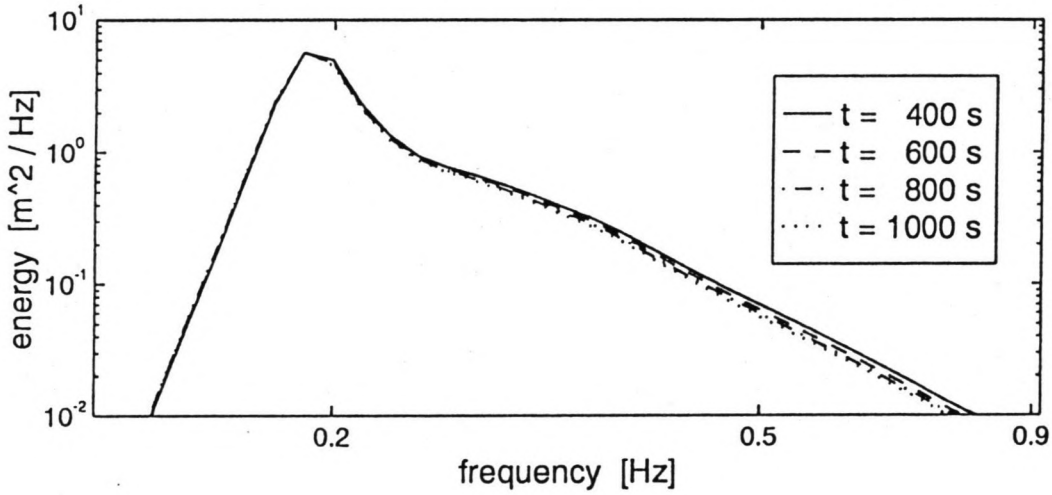

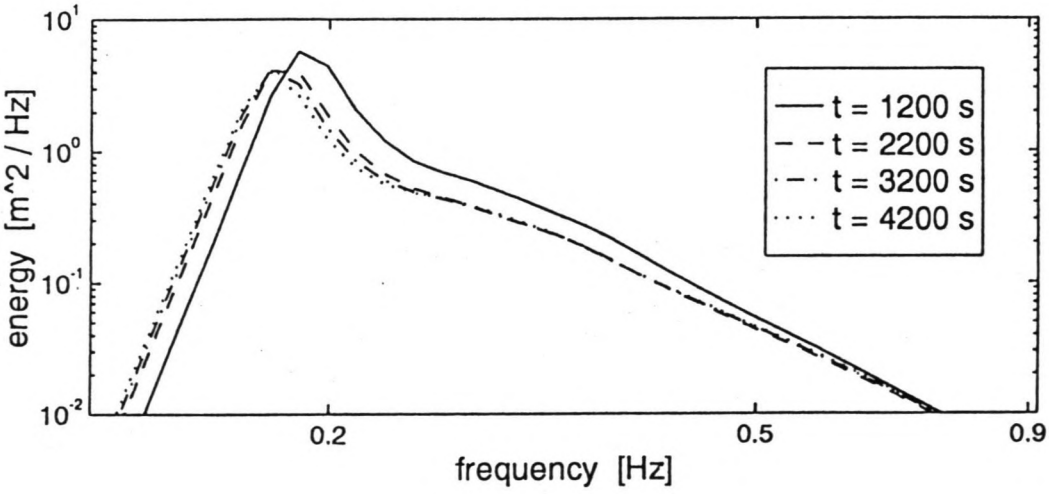

Figure 4.5 Spectra run 8 on logarithmic scale

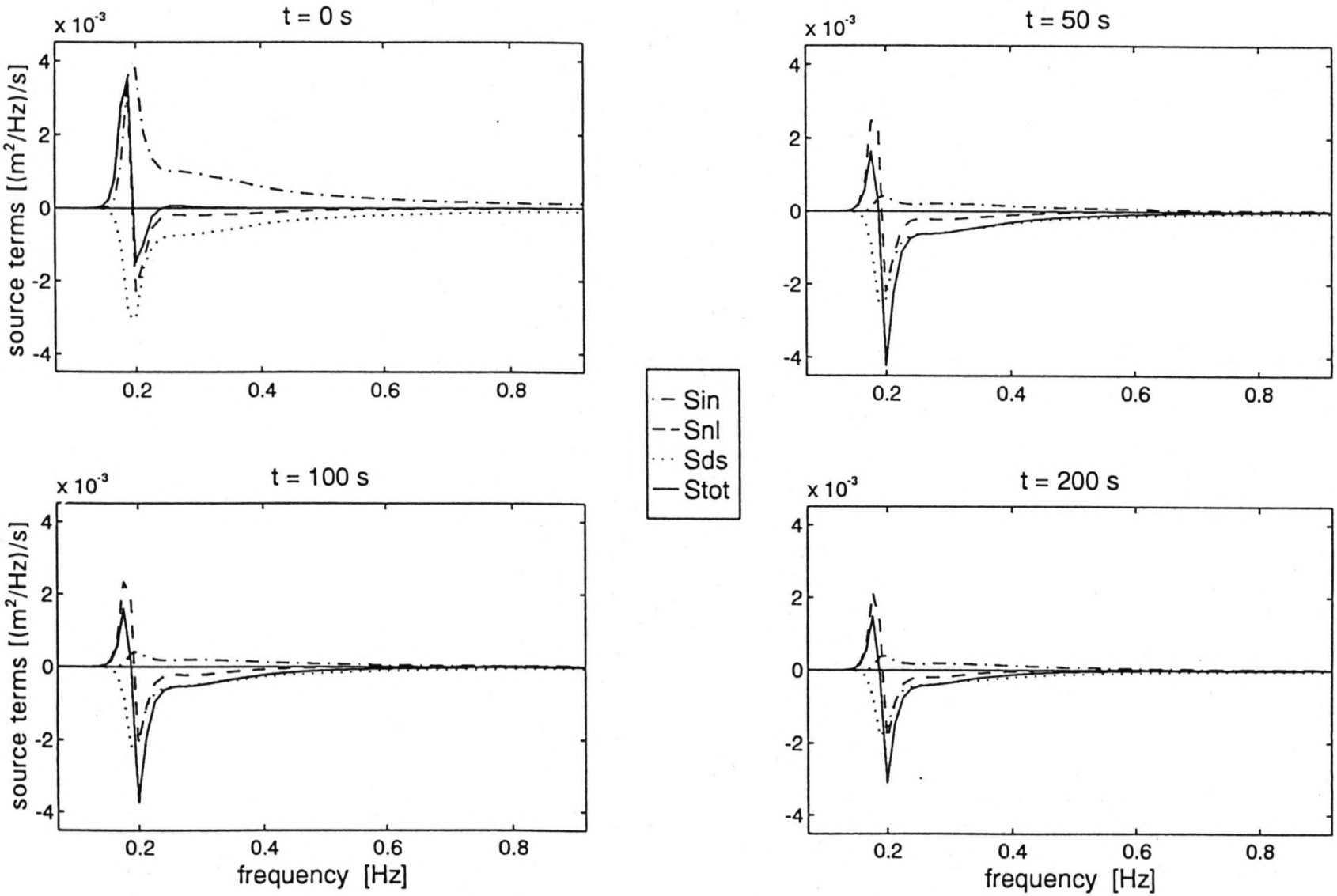

Figure 4.6 a Source terms run 8 (t = 0, 50, 100, 200 s)

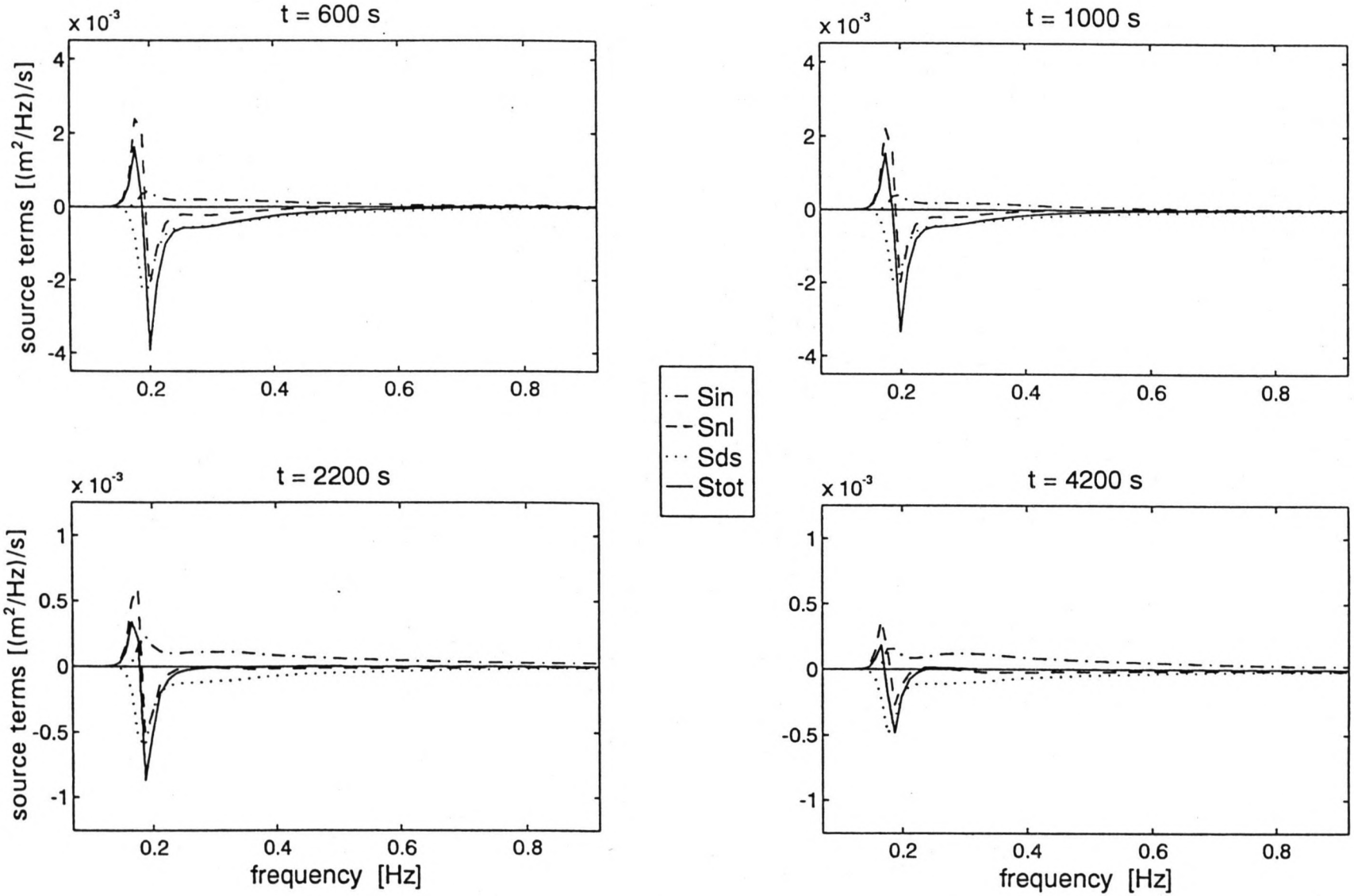

Figure 4.6 b Source terms run 8 (t = 600, 1000, 2200, 4200 s)

4.3 Rate of response of spectral components

Because the high frequencies respond most rapidly to a change in wind speed, they are most interesting for this study. Hence the further analysis in the following paragraphs considers frequencies above 0.3 Hz. This frequency is larger than the peak frequency in all runs.
In the figures 4.7 and 4.8 the dimensionless energy density E^* has been plotted as a function of time and frequency for run 2 and 8, where E^* is the energy scaled by the energy at t=0, $E_0(f)$.

$$E^*(f,t) = \frac{E(f,t)}{E_0(f)} \tag{4.1}$$

In these figures it can be seen that the high frequencies respond faster than lower frequencies. To get a better understanding of the general trends in the different runs, a simple equation was searched for to describe the response of the spectral components. A good fit was found with an exponential equation (see figure 4.9).

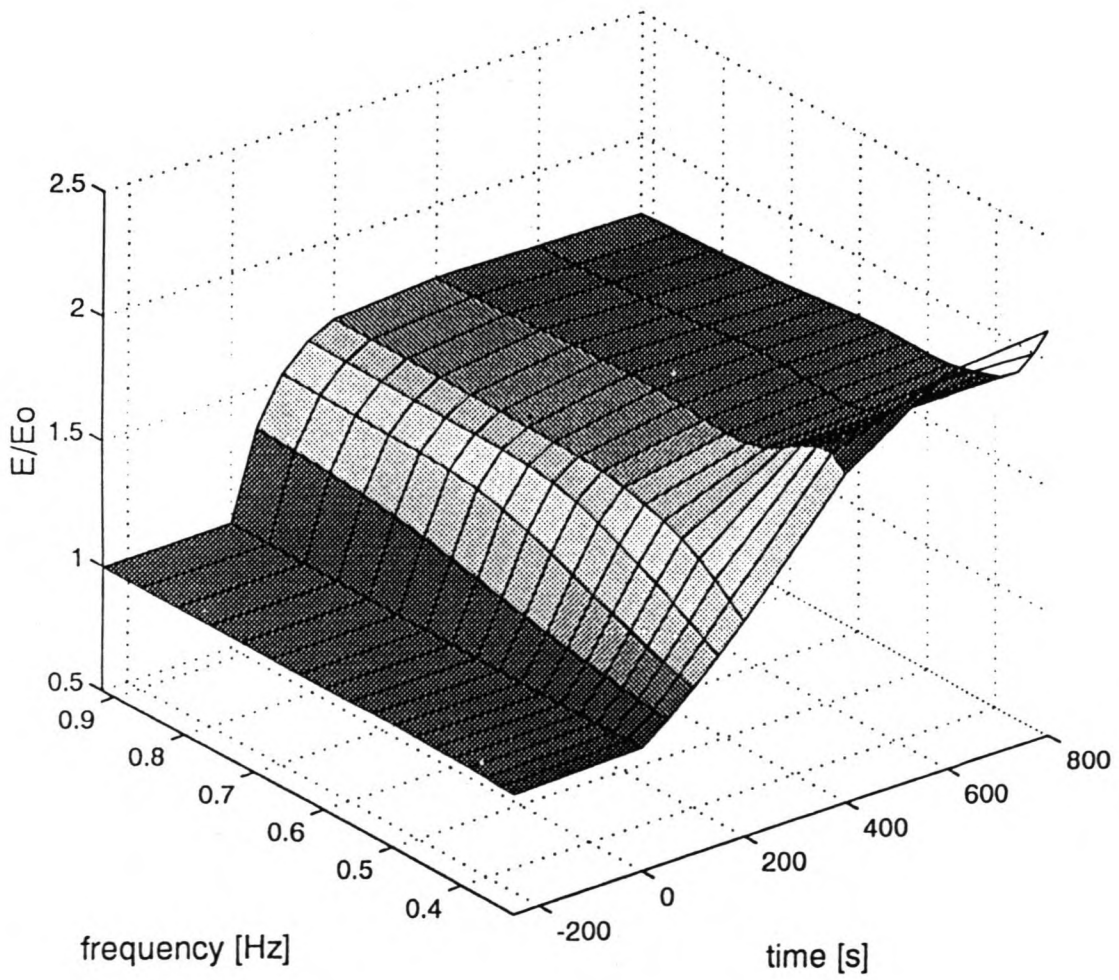

Figure 4.7 Non dimensional energy run 2

The following equation was formulated

$$E^*(f,t) = (1-E_e^*)e^{\pm\left[\frac{a}{1-E_e^*}\right]t} + E_e^* \tag{4.2}$$

where $E_e^* = E_e^*(f,\Delta U)$ is the dimensionless energy in the new equilibrium (for $t = \infty$) and $a = a(f,\Delta U,f_{p1,2})$ is a measure for the rate of response of a spectral component. To get positive values for a for both increasing and decreasing wind speed the plus sign should be used in case of increasing wind speed, for decreasing wind speed the minus sign should be used.
E_e^* can easily be estimated from the model results.

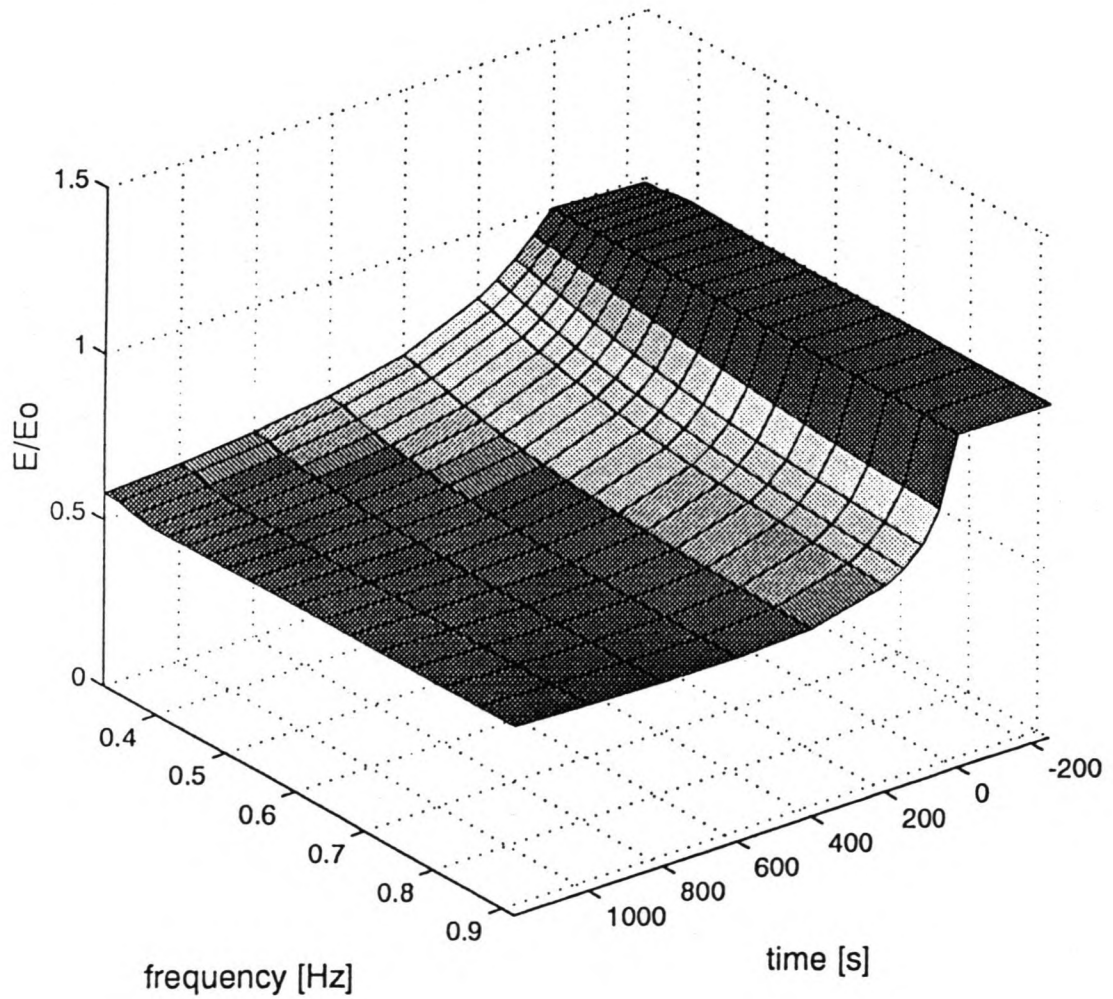

Figure 4.8 Non dimensional energy run 8

The time-derivative of equation (4.2) yields

$$\frac{\partial E^*}{\partial t} = \pm a e^{\pm\left(\frac{a}{1-E_e^*}\right)t}$$

which shows that at t = 0 the rate of response of a spectral component is equal to a. So comparing the value of a for different frequencies or situations is interesting for analysing the rate of response of a spectral component immediately after a sudden change in wind speed.
The value of a was determined by using a least square method. In figure 4.10 the results for a for increasing wind are shown. The figures show an increasing value of a for increasing frequencies, indicating a faster response of the high frequencies. Comparing the value of a for different increase in wind speed, a faster response for a larger increase is found.

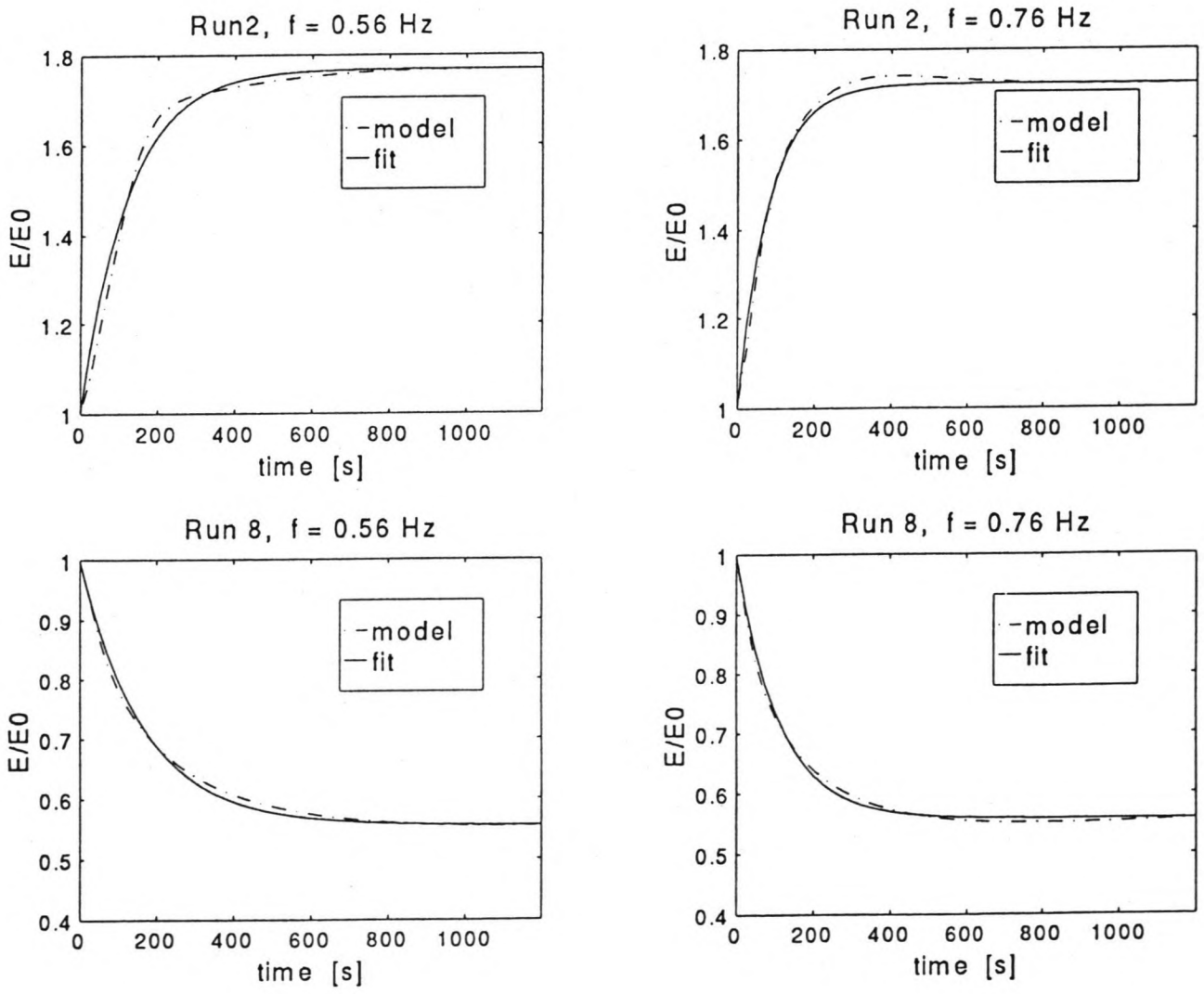

Figure 4.9 Examples of fits with an exponential function

For a decreasing wind speed a shows the same trend (see figure 4.11), an increasing value of a for increasing frequency. The variation of a for different ΔU does not follow a logical trend. This may be caused by the fact that especially in the case of $\Delta U = 5$ m/s the used equation does not give a very good fit. The runs 7, 8 and 9 were performed starting with a peak frequency of 0.19 Hz, a little developed spectrum for the wind speed of 20 m/s. Even for a wind speed of 15 m/s (run 7) this is not a fully developed spectrum. In this run the high frequencies first lose energy, but soon the source terms balance again and the spectrum even starts growing despite the smaller wind speed. In run 9, $\Delta U = 15$ m/s, the total source term stays negative until the end of the calculation ($t = 4200$ s).

A significant result is that for increasing wind speed the values of a are almost the same for the two different peak frequencies, so in these cases the response of the high frequencies seems to be independent of the rest of the spectrum. However for decreasing wind a is larger for the runs with the larger peak frequency. So if the spectrum has less developed, it adjusts faster to new circumstances than in case of a more developed sea.

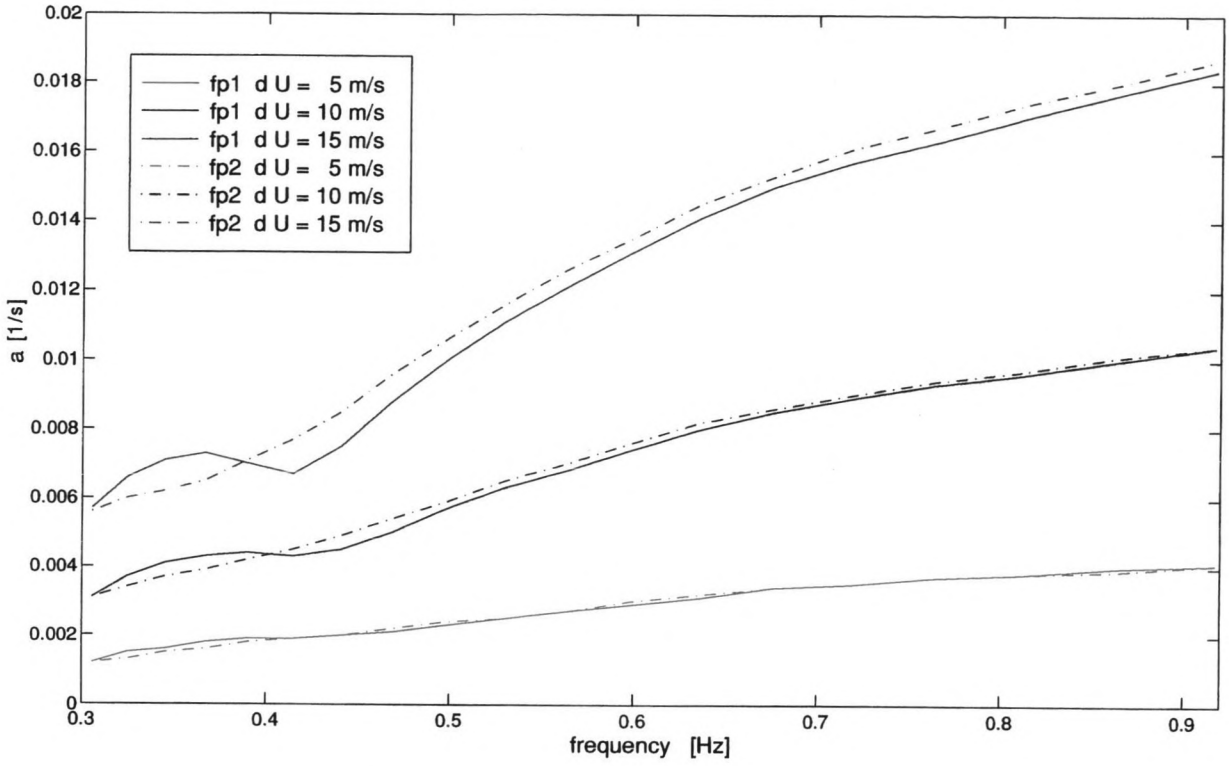

Figure 4.10 a for increasing wind speed

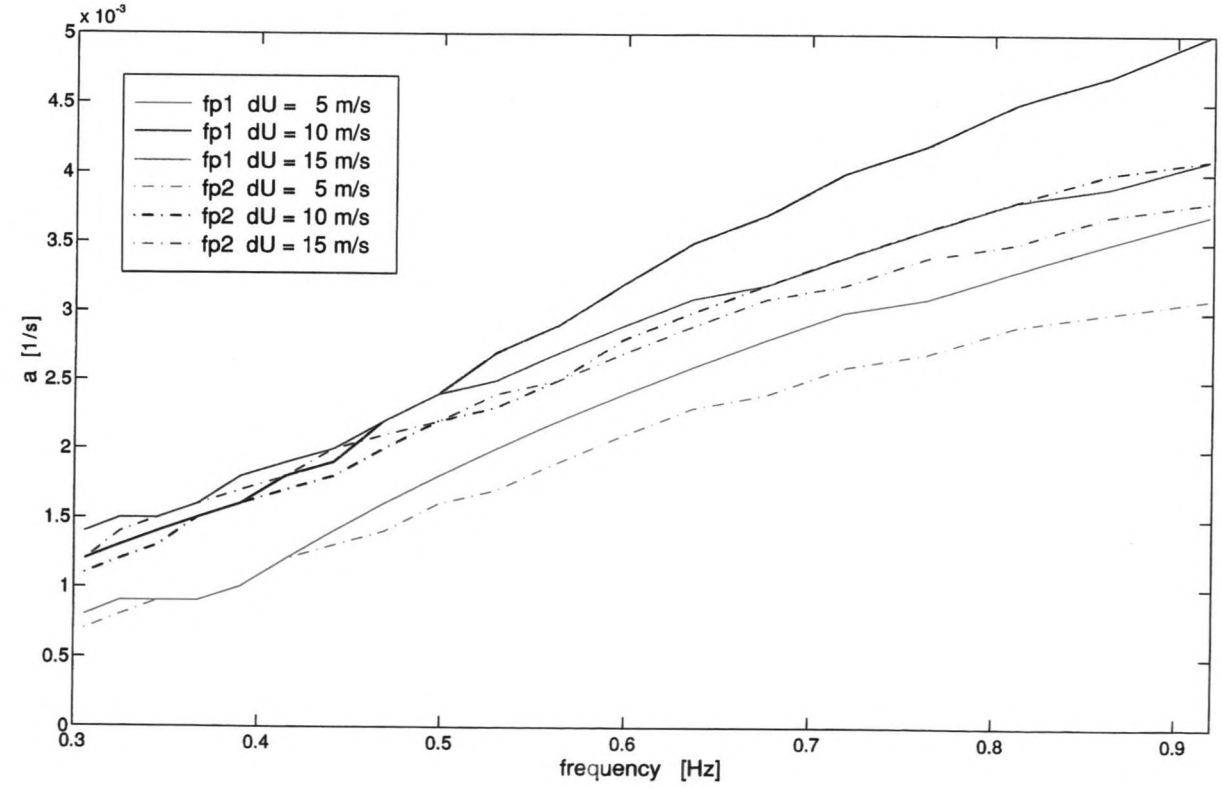

Figure 4.11 a for decreasing wind speed

Another way to obtain more insight into the model behaviour is by looking at $t_{½}$, the time needed to reach an energy density of $½(E_0^* + E_e^*)$. This gives information about the rate of adjusting to a new equilibrium, in contrast to *a*, which is the adjustment rate immediately after a change in wind speed.

In figure 4.12 $t_{½}$ was plotted as a function of f for all runs with increasing wind speed, in figure 4.13 for decreasing wind speed. From the figures it is clear that the high frequencies adjust faster to a new equilibrium than low frequencies, both for increasing and decreasing wind speed.

For increasing wind speed $t_{½}$ increases with decreasing ΔU, so the process is slow for a small increase in wind speed. Although E_e^* is larger for larger ΔU, $½(E_0^* + E_e^*)$ is reached earlier because the input of energy increases even more.

For decreasing wind speed the opposite happens. Now the process is slower for a larger decrease in wind speed. As explained before, in run 7 the high frequencies do not lose much energy and reach a new equilibrium level quickly, while in runs 8 and 9 the spectrum must lose much more energy which takes more time.

The curves for $t_{½}$ for the different initial peak frequencies are almost equal for increasing wind speed. For decreasing wind speed $t_{½}$ is larger for the runs 11, 12 en 13. These runs started from a more developed spectrum, so more energy must be dissipated before a new equilibrium is reached, which takes more time.
$t_{½}$ is of the same order of magnitude for increasing and decreasing wind speed, in contrary to *a* which is larger for increasing wind speed. So the initial response of the waves to an increase in wind speed appears to be faster than the response to a decrease in wind speed, but a new equilibrium is reached in about the same time.

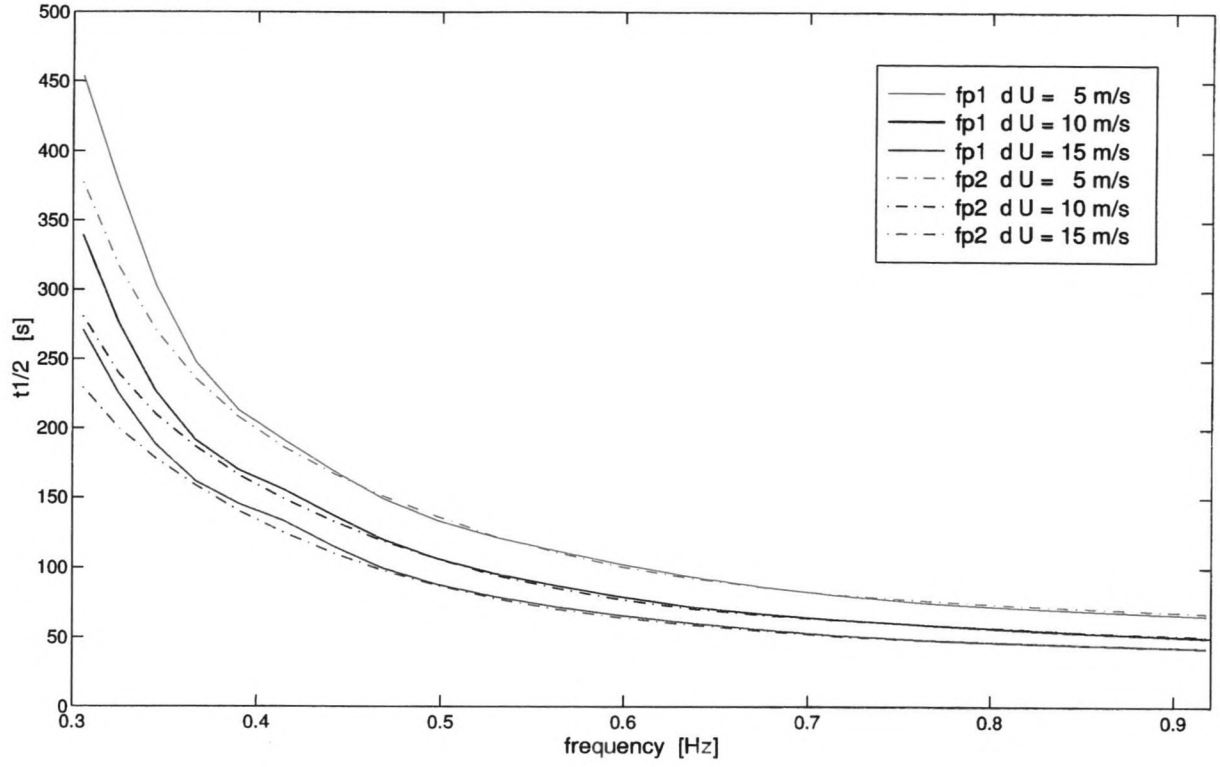

Figure 4.12 $t_{½}$ for increasing wind speed

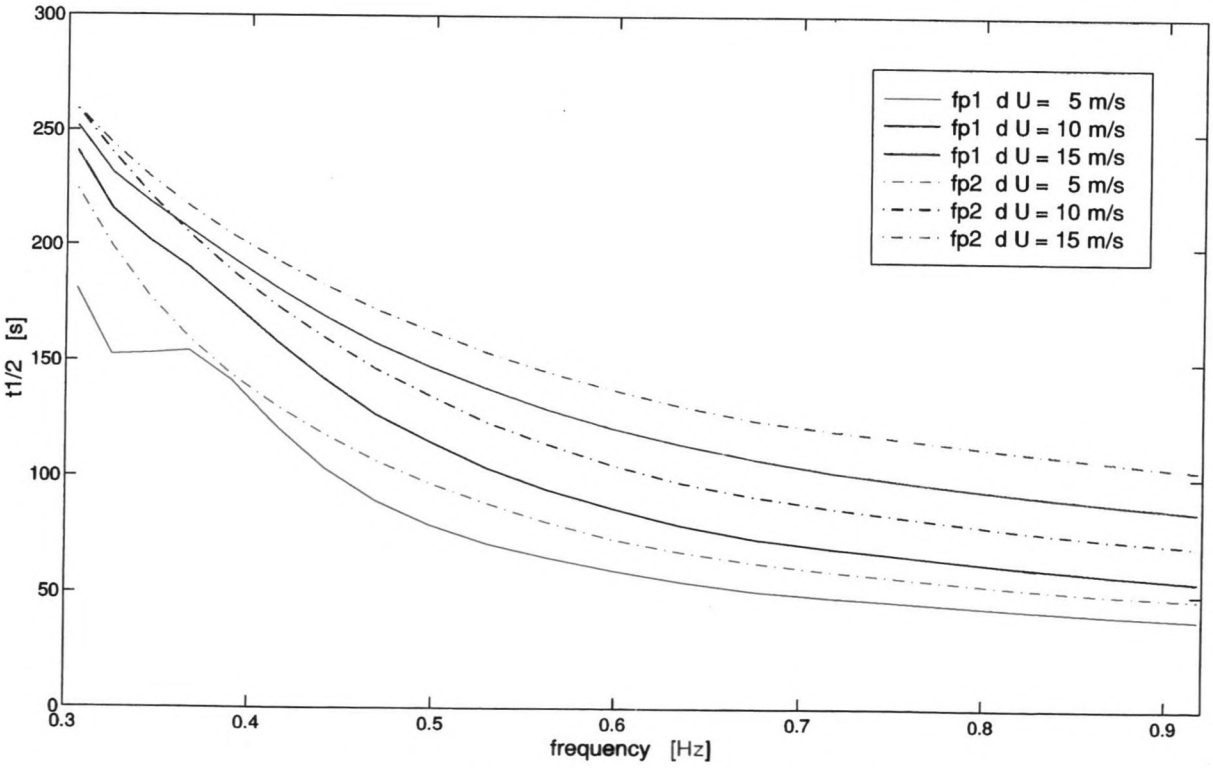

Figure 4.13 $t_{½}$ for decreasing wind speed

5. Field Measurement Instruments and Procedure

5.1 The equipment on Lake George

The field measurements for this study were carried out on Lake George as a part of a large wave measuring project of the University of New South Wales started in 1991.
Lake George is situated about 50 kilometres North East of Canberra (Australia), see figure 5.1. It has a length of approximately 20 kilometres and is about 10 kilometres at its widest point.
It is filled by precipitation and three brooks discharge into the lake at the east side.

The water level of the lake shows very large fluctuations. The lake has reached depths of over 7 meters and has fallen dry as well. Over recent years the mean depth has been approximately 1.7 meter with a variation of 0.4 meter.

Figure 5.1 Australia

As the measuring project on Lake George has already been working for two and a half years, the choice or design and location of the equipment was fixed. At the lake 8 framework towers (see figure 5.2) for the measuring equipment were built along the north-south axis (see figure 5.3).

Figure 5.2 One of the measuring stations

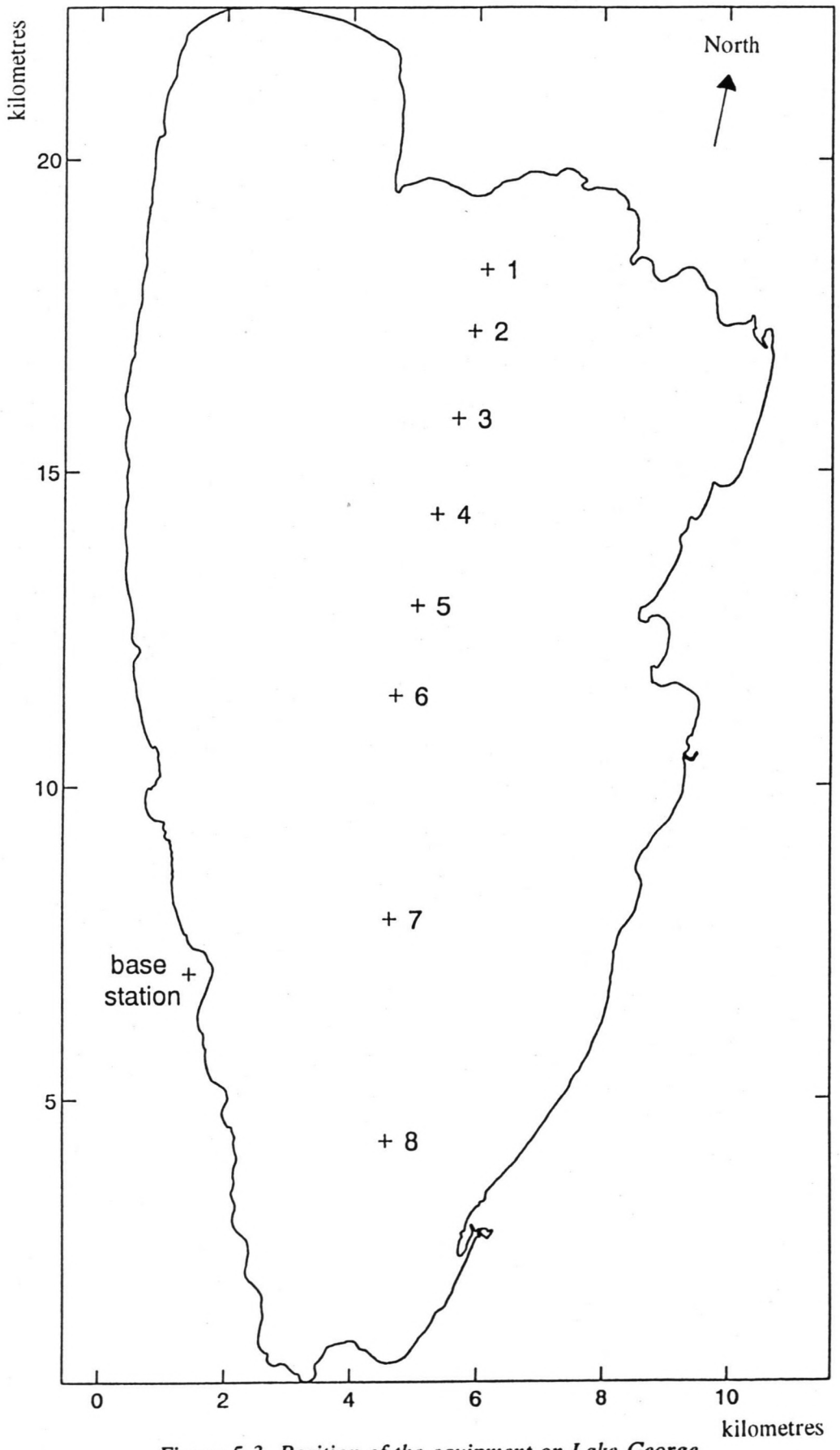

Figure 5.3 Position of the equipment on Lake George

At each of the stations a wave gauge has been installed. More information about the wave gauges can be found in the next paragraph.
At 5 of the stations (2, 4, 6, 7 and 8) the wind speed and direction is measured at 10 meters above the water surface. At station 6 a R.M. Young propeller anemometer is used, the other stations have VDO cup anemometers.
At the stations 2, 4, 7 and 8 the wind data is registered with a data logger and must be collected on the spot once a month. The wind data of station 6 is transmitted to the base station on the shore by a radio at a sampling frequency of 0.83 Hz.
The energy for the instruments is obtained by solar panels. The solar energy feeds batteries which collect enough energy for nightly supply.

In cooperation with the Bureau of Meteorology in Melbourne the water temperature at the surface, middle and bottom, the air temperature and humidity are measured at the stations 2, 6 and 8. At station 6 the Bureau of Meteorology also has a radiation meter, which measures the net radiation just above the water level, giving a measure for the amount of radiation energy transported from the atmosphere to the water.

Figure 5.4 The platform at Lake George

Station six has, except for the tower, a platform (see figure 5.4) which functions as a base for additional experiments. Near the platform an array of 7 wave gauges was placed to measure directional spread. The platform is equipped with a shed with a computer, among others to operate the array. Recently also a hydrophone was installed here for an experiment to investigate the relation between the dissipation of wave energy and the noise made by breaking waves. This is a future project, for which also video equipment will be used to record optical data about wave breaking.

5.2 The wave gauges

The wave gauges are Zwarts poles (Zwarts, 1974), working on the following principle.
A gauge consists of an inner and outer pole. The outer pole has holes all around, so the water level between the inner and outer pole follows the water level outside (see figure 5.5). At the top of the pole is a little box, from where an electromagnetic wave is sent through the inner pole towards the water level. Between the box and the water level a standing wave is formed. From the wavelength of this standing wave the distance between the top of the pole and the water surface can be derived. In this way the wave height is determined at a frequency of 8 Hz.

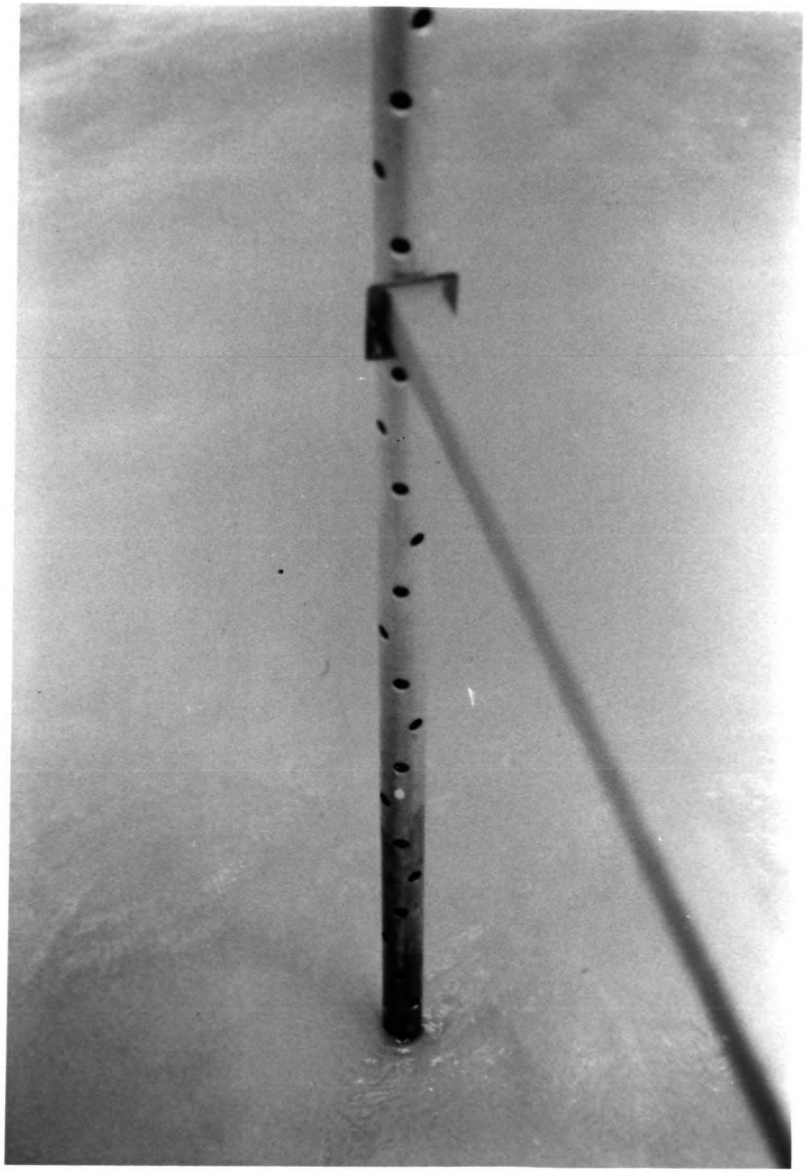

Figure 5.5 Zwarts pole

To be able to check the data for transmission errors, the Zwarts poles have a counter card, counting at the same frequency of 8 Hz. By gaps in the sequence count transmission errors can be detected.

The advantages of Zwarts poles are that they require little maintenance and the calibration is valid for a long time, in contrast to capacity and resistance wave gauges. In addition, they are rugged and not easily damaged.

The measured wave data is transmitted to the base station on the shore by radios. At the base station two computers log the data received by the radios (see figure 5.6). The data is logged during half an hour every hour, except for pole 6. For the purpose of this study, looking at changing wind situations, it is better to have continuous time series. So the logging procedure of this gauge was changed in continuous data logging. For the logging of the data a real-time program has been made which stores the data in files, separate files for wind and wave data, each file containing the measured data of one hour.

Figure 5.6 Receiving radios at the base station

5.3 Field Work

The measuring of wave and wind data occurs fully automatically and continuously, except the array of wave gauges, which is only operational when interesting weather conditions are expected. (The data logging of these poles can be switched on via the modem at the university.) This does not mean that everything can be done sitting behind your desk at the university. There is still a lot of field work to do to keep the system working. The author assisted in all activities mentioned below.

The only routine work that had to be done was to get the measured data from the temporal storage at the base station to the university. This was done by copying the data from the two personal computers at the base station (see figure 5.7) to two portable computers. The hard disks were full within ten days, so this meant a drive to the base station very regularly (including a meeting with the dangerous 'killer cow' in the paddock where the base station is situated).

Figure 5.7 The base station

In addition the data for the Bureau of Meteorology must be collected from the data loggers once a month. This was considerably more time consuming, because these data loggers were situated at the stations on the lake itself. For the purpose of going to the lake the university owns a little power boat. All work on the lake was preferred to be carried out on calm days, because a lot of time could be saved sailing on the lake without the choppy waves at windy days.

Another aspect of the field work was all kind of maintenance activities. An example is the replacement of the batteries at each station by new ones. A large operation was the cleaning of the gauges from algae, which could hinder the water running into the holes of the poles. To clean the poles they had to be dismantled which requires scuba diving to undo the bolts under water (see figure 5.8). Other hindrance by animals was the bird droppings on the solar panels. So these had to be cleaned once in a while. To avoid this, sharp metal points were placed at the top edge of the solar panels.

Figure 5.8 Installing the Zwarts poles of the array

Besides the above activities an aspect of the field work not to be underestimated concerns repairing things. When (a part of) the complex system is not working, the most difficult task is to find out what is wrong. Often the broken link has to be found by trial and error. A few examples are given below.

One day the radios used to transmit the data to the base station were brought to the university to tune them, just for preventive maintenance. After bringing them back to the lake the reception of the radios appeared to be worse than before, giving much more transmission errors. What was wrong ? It could be a mistake at installing the radios, or the new car-telephone mast, interfering at the frequencies of the radios, but theoretically everything could have been broken coincidentally.

Finally the radios were taken from the lake again and brought to the factory in Sydney, where they found out that the tuning was wrong.

A thunder storm was nearly always a reason for at least one of the stations to stop working. Putting the switch on the electronics board off and on again, usually worked to restart the data transmission. As the switch is located at the station itself it asks a lot of time for only pressing a button.

Other things to repair incidentally were oblique aerials and wind vanes, caused by wind or pelicans.

5.4 Wind data analysis

The wind data consists of two parts, wind speed and direction, both measured at a level of 10 meters above the water surface at a frequency of 0.83 Hz and stored in files of one hour. To make these data suitable for general processing, transmission errors (e.g. unintentional received data) have to be repaired first. This was done by a kind of filtering program.

For the presentation of the wind data in this report the data is averaged over about 1 minute (50 sample points). The average wind direction has been calculated in two ways. The first method uses equal weights for every sampled wind direction, in the second method the wind direction is first multiplied by the wind speed before averaging. In most cases this does not make a significant difference. The average wind direction cannot be calculated in a straightforward summation and division, because this gives a problem for wind directions around zero. For instance one sample point with a direction of 2° and another of 358° would give an average direction of 180°. This problem is removed by decomposition of the wind direction into two perpendicular vectors.

To obtain data suitable for this study out of the large amount of measured data, all data has first been checked for the range in wind speed within one file. The files with a range in wind speed of more than 6 m/s were selected.
A second selection criterion is the wind direction. Only files with a wind direction that does not deviate by more than 30° from the average direction have been used. This criterion reduces the amount of data considerably, because most changes in wind speed come together with a large change in wind direction.
It appeared that generally an increase in wind speed occurs much faster than a decrease. Because very slow decreasing wind is not very interesting for this study, there is not much useful data of decreasing wind.

An interesting fact is that nearly all cases with a significant increase in wind speed happened at about 17.00 h with wind coming from the east. This is caused by the rising of the air above the land surface heated during the day and the cooler air from the above the sea coming inland. This phenomenon is clearly visible at Lake George although the sea is about 125 km away.

5.5 Wave data analysis

The wave data matching the selected wind files has been subjected to a wave analysis program doing the following two things. First it checks the data for transmission errors. When a file contains too many errors the data is rejected, a limited number of errors is accepted, but mentioned in the output. The wrong data points are replaced by dummies.

Second the program calculates the spectra with a Fast Fourier Transform (FFT) procedure. FFT procedures were introduced in 1965. Previous methods of Fourier transforms were very time consuming. Usually first an auto-correlation function was calculated. The spectral density was estimated by the Fourier transform of the correlation function. FFT procedures estimate the spectral density directly from the time record.

Algorithms for Fourier transforms are based on the following principle. Assume a sample record x(t) sampled at N equally spaced timesteps Δt seconds apart

$$x_n = x(n\Delta t) \qquad n=0,1,2,3,\ldots,N-1 \tag{5.1}$$

For arbitrary f the discrete version of the finite-range of the Fourier transform of above equation is

$$\chi(f,T) = \Delta t \sum_{n=0}^{N-1} x_n \exp(-j2\pi fn\Delta t) \tag{5.2}$$

The usual selection of the discrete frequencies for the computation of χ(f,T) are

$$f_k = \frac{k}{T} = \frac{k}{N\Delta t} \qquad k = 0,1,2,\ldots,N-1 \tag{5.3}$$

Note that the results are only unique to k=N/2 because f=1/(2Δt) is the Nyquist frequency above which aliasing occurs.

Equation (5.2) combined with equation (5.3) yields

$$\chi_k = \frac{\chi(f_k,T)}{\Delta t} = \sum_{n=0}^{N-1} x_n \exp\left[-j\frac{2\pi kn}{N}\right] \qquad k = 0,1,2,\ldots,N-1 \tag{5.4}$$

To compute all of the χ_k terms involved, approximately N^2 complex multiply-add operations are necessary (1 complex multiply-add operation = 4 real multiply-adds).

FFT procedures are based upon decomposing N into its composite factors and computing the Fourier transforms over the number of terms of the composite factors. If N is the product of p factors

$$N = \prod_{1=1}^{p} r_i = r_1 r_2 \ldots . r_p \tag{5.5}$$

equation (5.4) can be found by the summation of

(N/r1) Fourier transforms requiring $4r_1^2$ real operations
(N/r2) Fourier transforms requiring $4r_2^2$ real operations
. . . .
. . . .
. . . .
(N/rp) Fourier transforms requiring $4r_p^2$ real operations.

Hence the total number of real operations becomes

$$4(Nr_1 + Nr_2 + \ldots\ldots + Nr_p) = 4N \sum_{i=1}^{p} r_i \tag{5.6}$$

The speed ratio to the standard Fourier transform is

$$speed\ ratio = \frac{4N^2}{4N \sum_{i=1}^{p} r_i} = \frac{N}{\sum_{i=1}^{p} r_i} \tag{5.7}$$

The speed can be enlarged when N is a power of 2. If $N = 2^p$ the exponential term of equation (5.4) is always +1 or -1. This results in doubling of the speed.

For the FFT of the wave analysing program, available software was used. The FFT was carried out for blocks of 256 sample points. As the sample speed was 8 Hz the Nyquist frequency is 4 Hz and the frequency resolution is 0.03125 Hz.
The reliability of the results was increased by averaging the spectra of 14 blocks, leading to spectra with 28 degrees of freedom.
One spectrum contains (14x256x0.125 s =) 7.5 minutes of data. This is relatively short, but necessary because of the non-stationary data.

Besides the estimates of the spectra the program calculates the significant wave height H_s and the 95 % confidence limits of both spectra and the significant wave height. The significant wave height is defined by the average of the highest third part of the waves, which can be approximated by

$$H_s = 4\sqrt{E_{tot}} \tag{5.8}$$

in which

$$E_{tot} = \int_0^\infty E(f)df \tag{5.9}$$

6. Comparison of Field Measurements and Modelling

6.1 Introduction

The most suitable data measured at station 6 (referred to as lake data in the following) was selected to be simulated with the two numerical models. These suitable situations can be divided in three categories: a sudden increase, a gradual increase and a gradual decrease in wind speed. In this chapter the lake data and numerical results are compared and significant results will be discussed.

With WAVEWATCH three runs for each case were made. In the first series of runs (WW-I) the calculations were made for an infinite large and deep ocean to compare these results with the results of Resio's model. The second series of runs (WW-II) takes the borders of the lake into account, but assumes the depth of the lake infinite to see the influence of the limited fetch. The bottom influence and fetch were taken into account in the last series (WW-III), which was carried out with a constant water depth of 1.8 m (approximately the average depth at the lake).

The values of a few important input parameters of the two numerical models are given in Appendix A.

The presentation of the lake data and numerical results is the same for all cases. Each case represents a period of one hour (t = 0 s to t = 3600 s). During the hour preceding the analysed one the wind speed was more or less constant with a speed the same as at t = 0 s. The figures consist of 5 parts: part *a* for the wind speed U_{10}, measured and model input; part *b* for spectra at 4 instants measured at the lake; part *c* for the measured and calculated significant wave height; part *d* for the peak frequencies (measured and calculated) and part *e* for the measured and calculated spectra at t = 3375 s.
The measured wave heights and spectra were calculated for each 7.5 minutes (see paragraph 5.5). The four instants of part *b* of the figures concern the intervals 7.5-15, 22.5-30, 37.5-45 and 52.5-60 minutes, referred to as t_1, t_2, t_3 and t_4. The spectra presented in part *e* of the figures are the spectra of the time interval 52.5-60 minutes, which are compared with model results at the midpoint of this interval (t = 3375 s).

6.2 Analysed cases

The fetch on the lake depends on the wind direction. Both wind direction and fetch of the five cases are given in table 6.1. The fetches are just short enough that the waves can be fetch limited instead of duration limited after one hour according to available nomograms. For instance the nomogram of Groen and Dorrestein (1976) gives for a wind speed of 10 m/s blowing for one hour, that the situation is fetch-limited if the fetch is shorter than 5 kilometres.

	case I	case II	case III	case IV	case V
wind direction	54°	88°	-71°	-72°	-96°
fetch	4.7 km	4.7 km	5.1 km	5.1 km	4.1 km

Table 6.1 Wind direction and fetch

The value of $k_p d$ (wave number at the peak frequency times water depth) was determined as a measure for the shallowness, see table 6.2. According to the classification by CERC (1984) water is considered deep for $k_p d > \pi$ and shallow for $k_p d < 0.25$. This means transitional conditions for the lake with frequencies around 0.4 Hz and a water depth of about 2 meters.

	case I	case II	case III	case IV	case V
$t_1 = 675$ s	5.14	2.61	1.78	2.26	1.13
$t_2 = 1575$ s	2.01	1.56	1.38	2.01	1.13
$t_3 = 2475$ s	1.48	1.16	1.10	1.42	1.13
$t_4 = 3375$ s	1.42	1.16	0.94	1.36	1.56

Table 6.2 $k_p d$

In the following the most significant features of the measurements and model results are treated per category (sudden increase, gradual increase and gradual decrease).

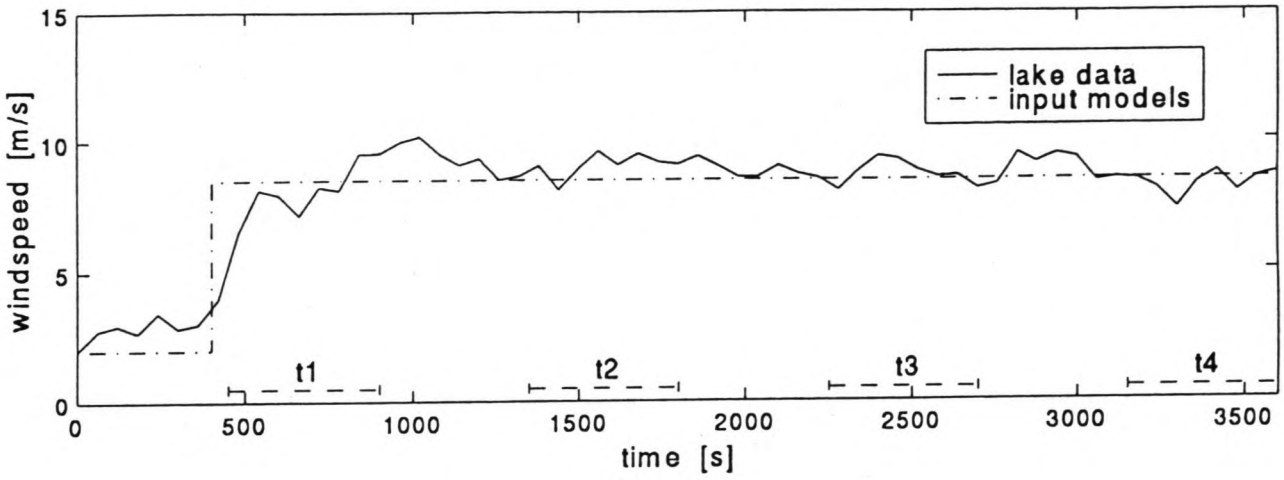

Figure 6.1 a Wind speed Case I

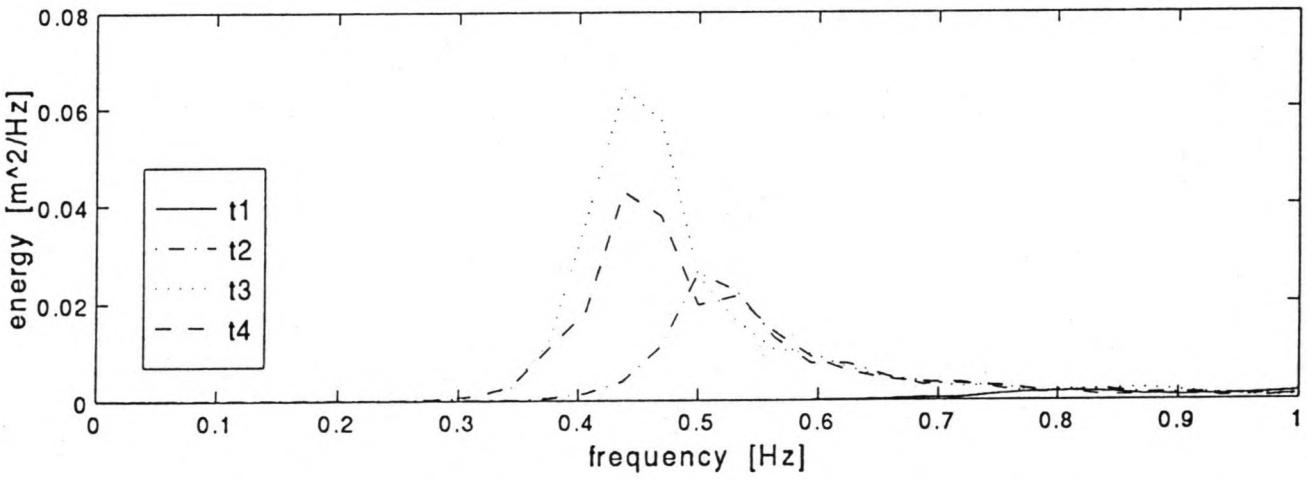

Figure 6.1 b Measured spectra Case I

Sudden increase in wind speed

Case I and II, two cases of a sudden increase in wind speed, are presented in the figures 6.1 a,b,c,d,e and 6.2 a,b,c,d,e. In case I the wind speed was simulated by a sudden change from 2 m/s to 8.5 m/s at t = 400 s, in case II from 3 m/s to 11 m/s at t = 250 s.
The significant wave heights of the lake data and Resio's model agree reasonably. The results of WAVEWATCH of H_s show that the influence of the limited fetch is small compared to the bottom influence. The WW-III results give a too small wave height.
Note that in figure 6.1 b the spectrum at t_3 is larger than at t_4. This unexpected fact can be explained by the slightly smaller wind speed at t_4. It is a significant fast response to the relatively small decrease in wind speed.
The figures 6.1 c en 6.2 c show that the peak frequency of the lake data moves quicker to lower frequencies than the peak frequency of the models.

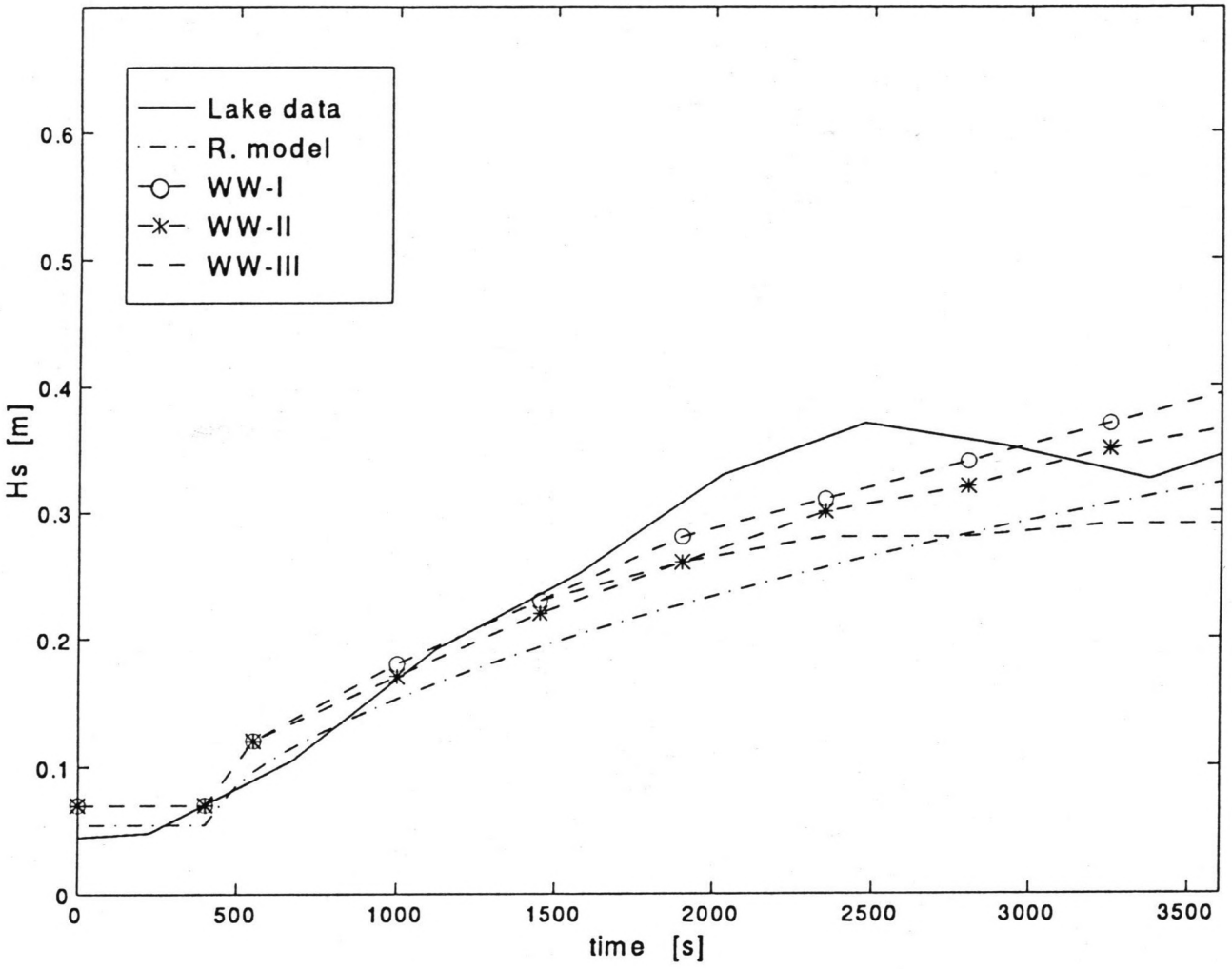

Figure 6.1 c Significant wave height Case I

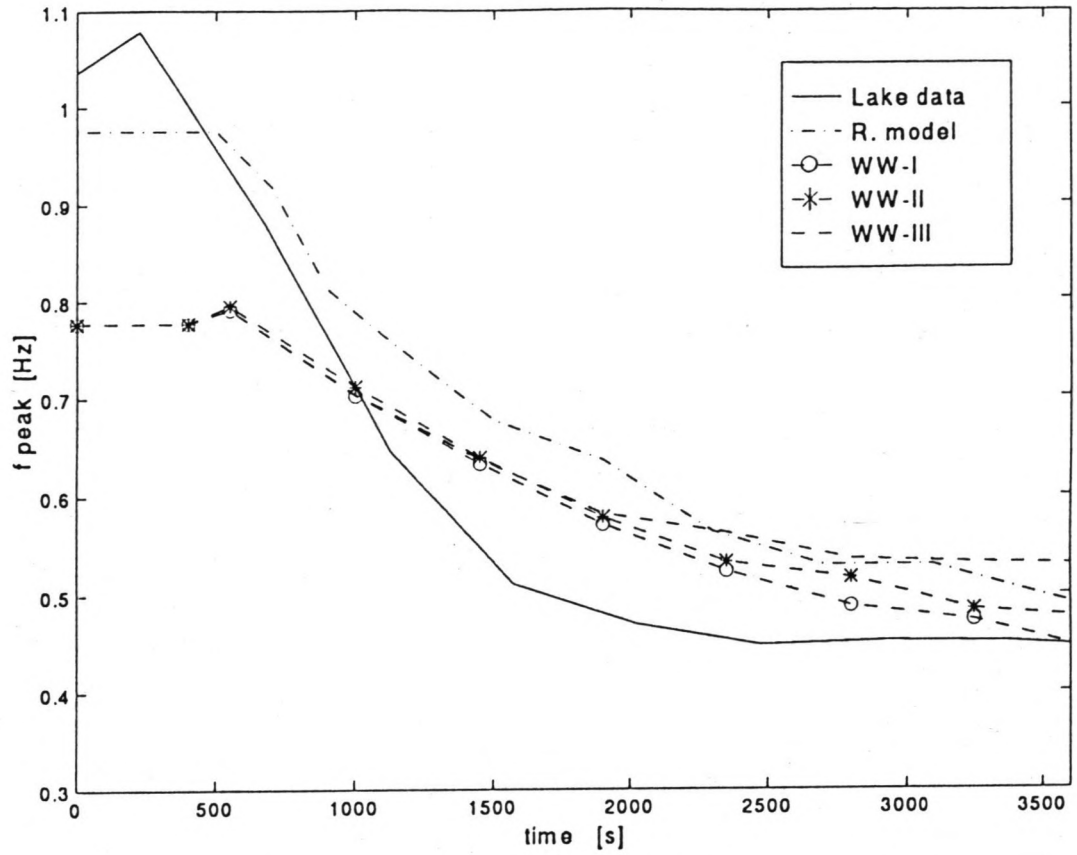

Figure 6.1 d Peak frequency Case I

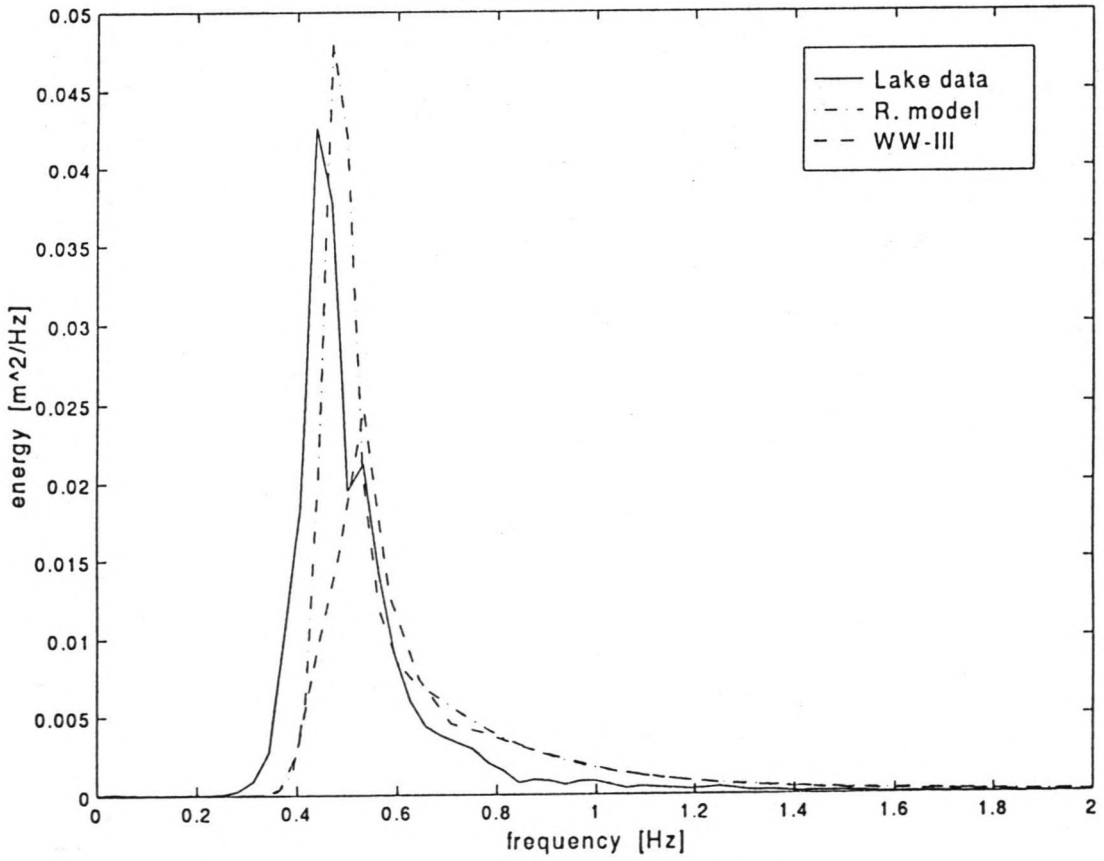

Figure 6.1 e Energy spectra at t_4 Case I

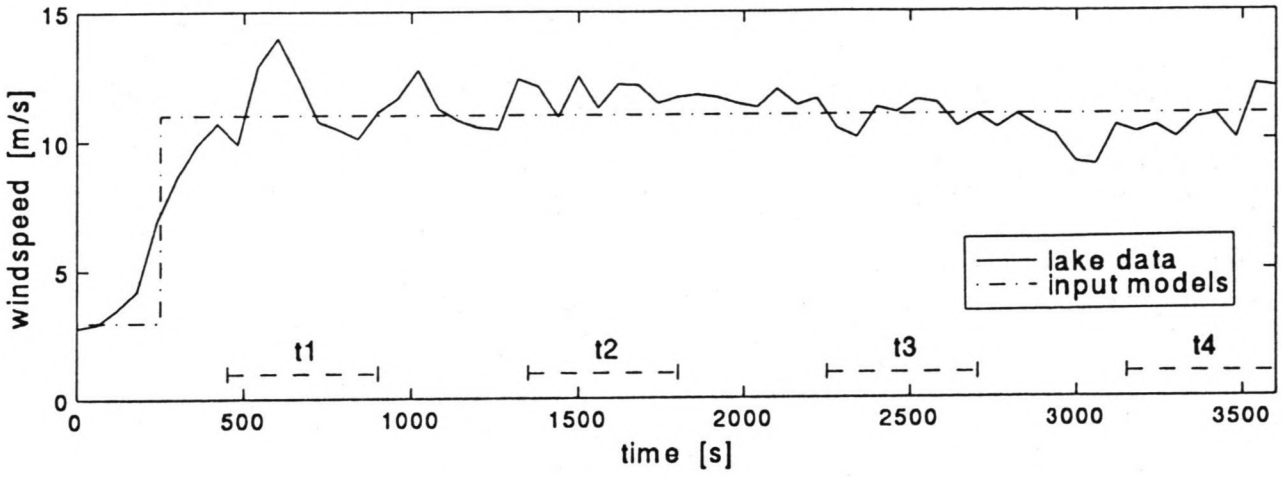

Figure 6.2 a Wind speed Case II

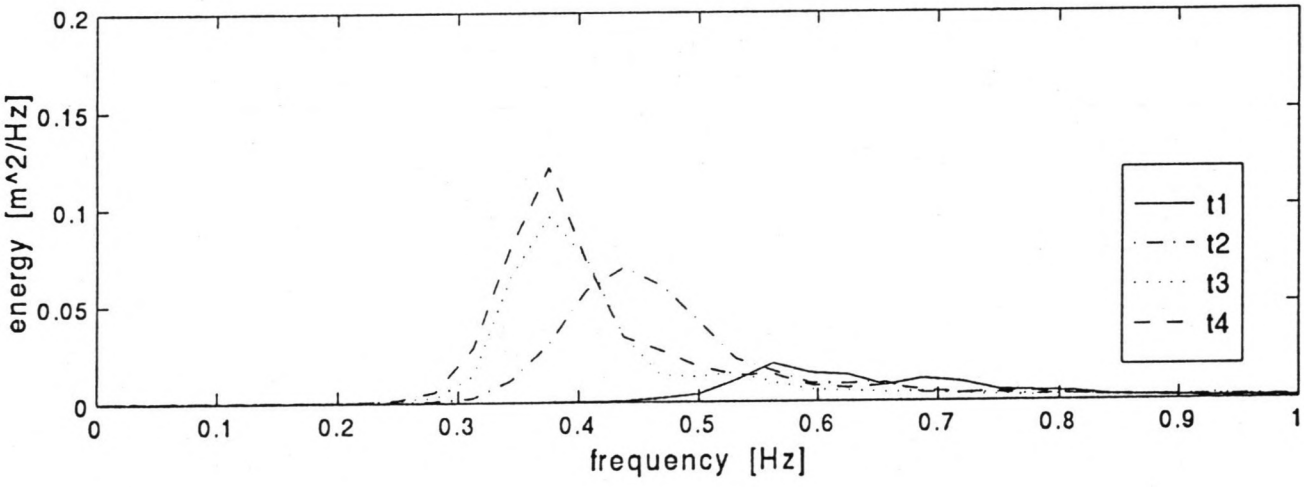

Figure 6.2 b Measured spectra Case II

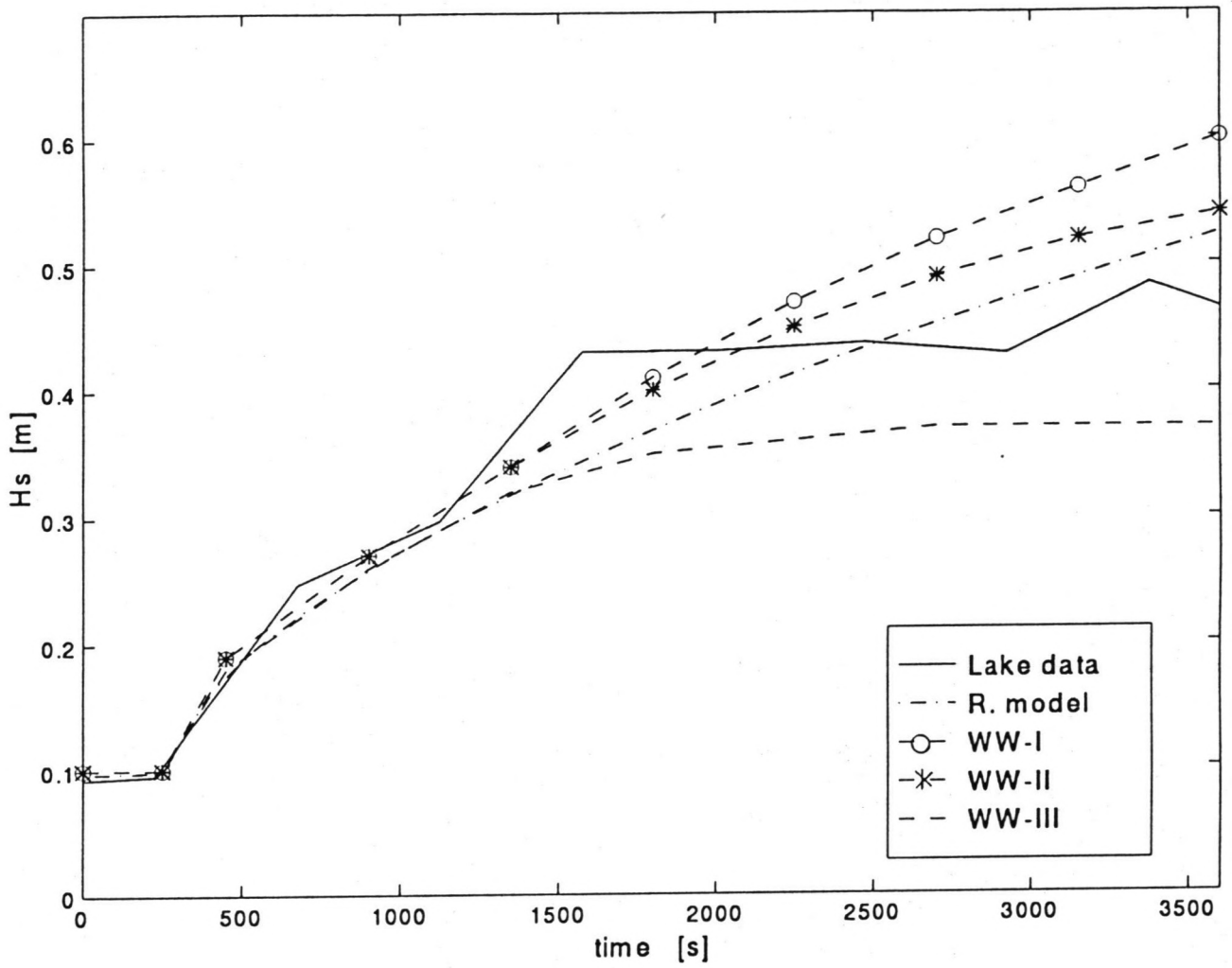

Figure 6.2 c Significant wave height Case II

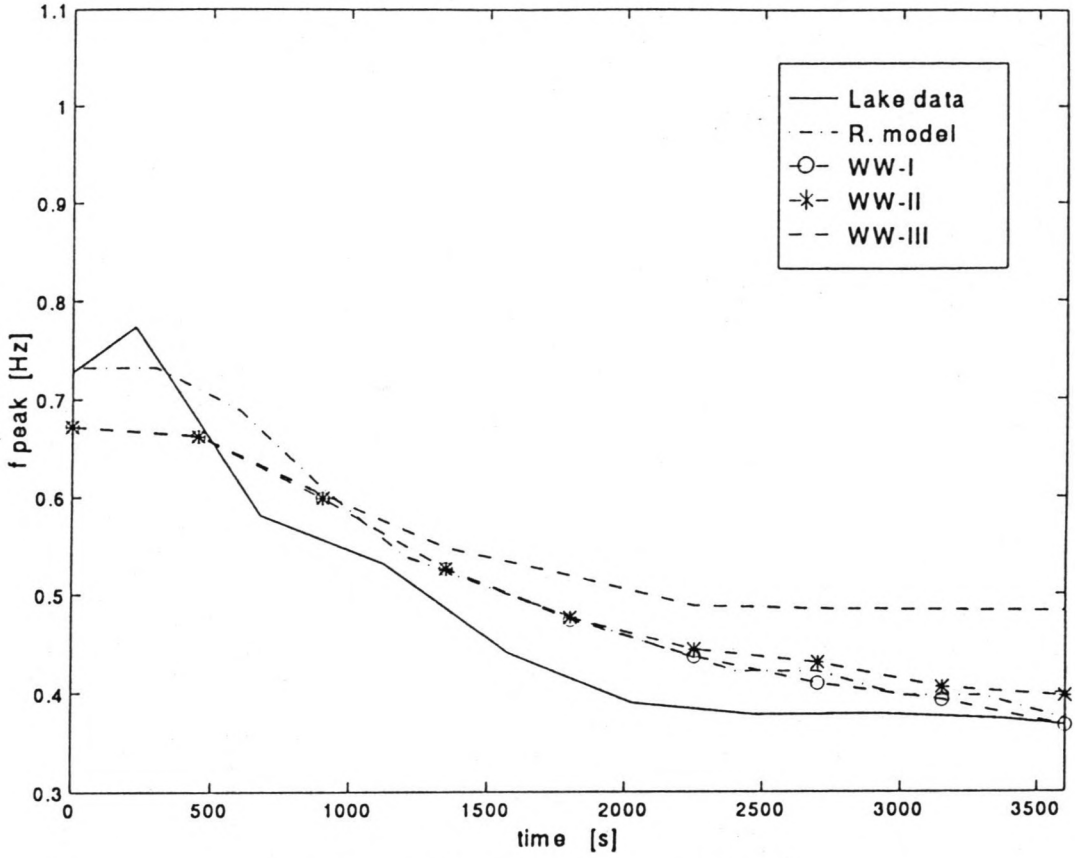

Figure 6.2 d Peak frequency Case II

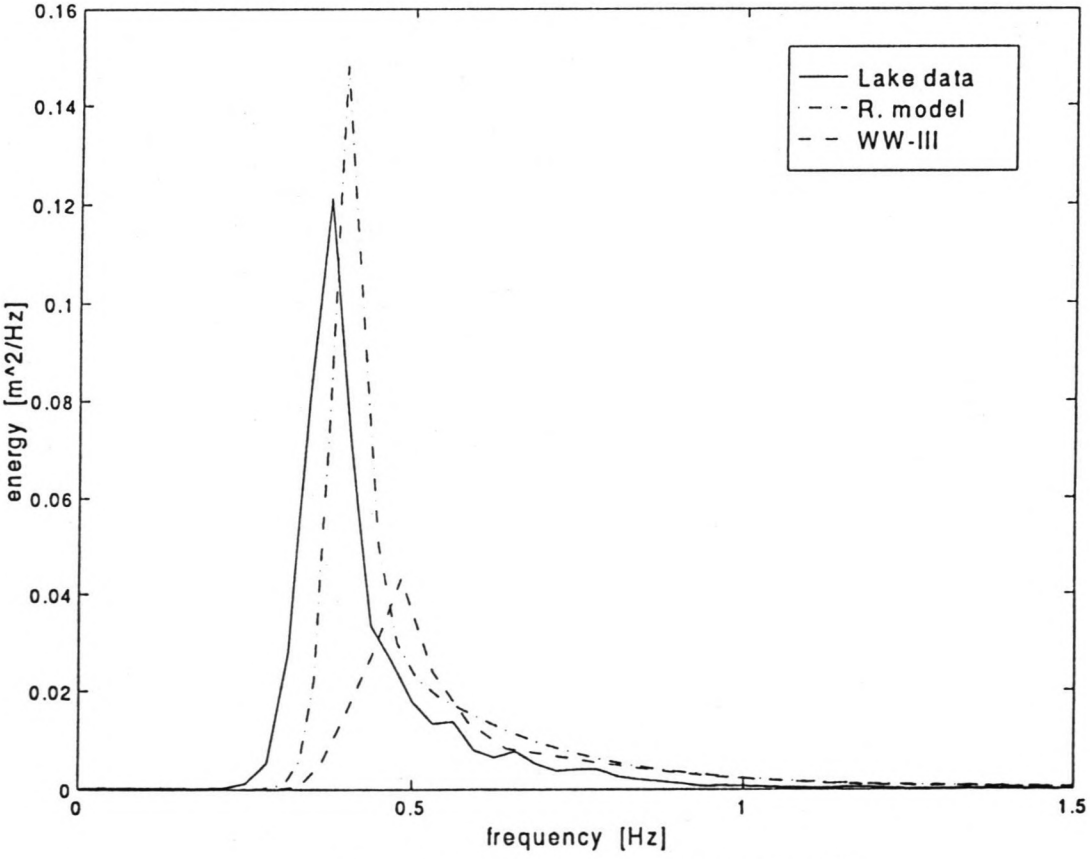

Figure 6.2 e Energy spectra at t_4 Case II

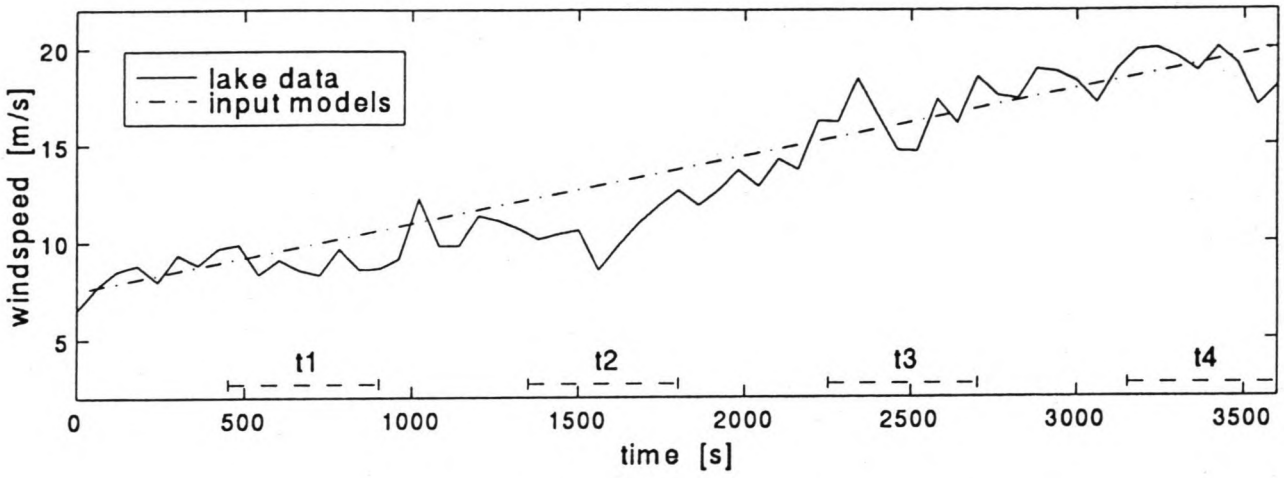

Figure 6.3 a Wind speed Case III

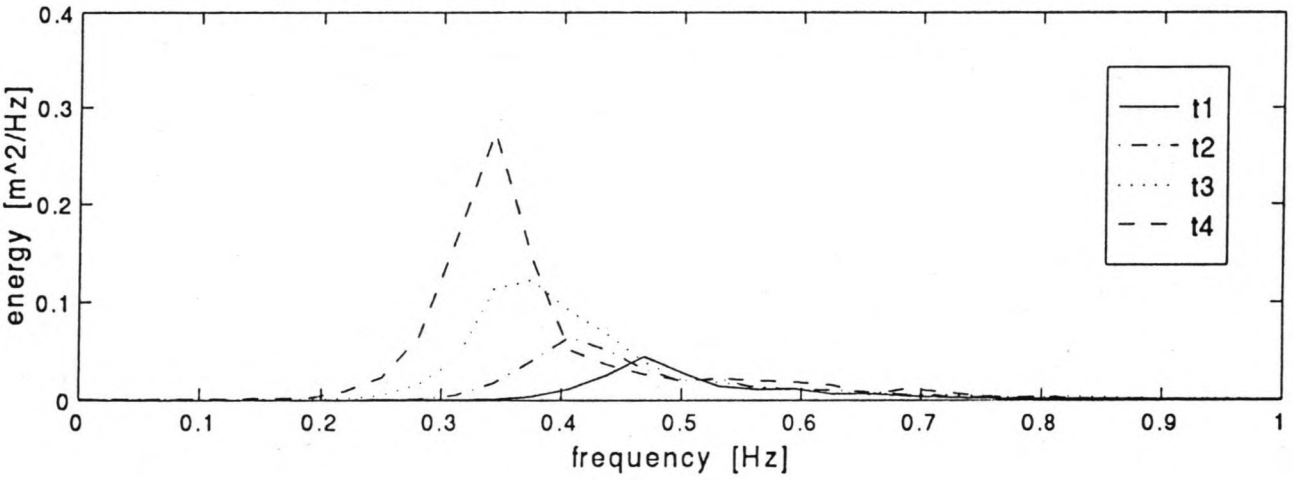

Figure 6.3 b Measured spectra Case III

Gradual increase in wind speed

Two suitable cases with gradually increasing wind speed were measured. These cases, III and IV, are shown in the figures 6.3 a,b,c,d,e and 6.4 a,b,c,d,e. The wind speed grows from 7.5 m/s to 20 m/s in case III and from 8 m/s to 17 m/s in case IV. For the wind speed in the models a linearly growing wind speed was used.

The wave heights of both cases show that in the model calculations without bottom friction the waves grow faster than in reality. So in contrast to case I and II now the bottom friction plays an important role. In case III, where the wind speed is larger than in case IV, the differences are considerable. The waves on the lake finally reach a significant wave height of about 0.7 m. This is very large in about 2 m water depth. When the bottom friction is included in WAVEWATCH (WW-III) the significant wave height is too small and the peak frequencies are too large.

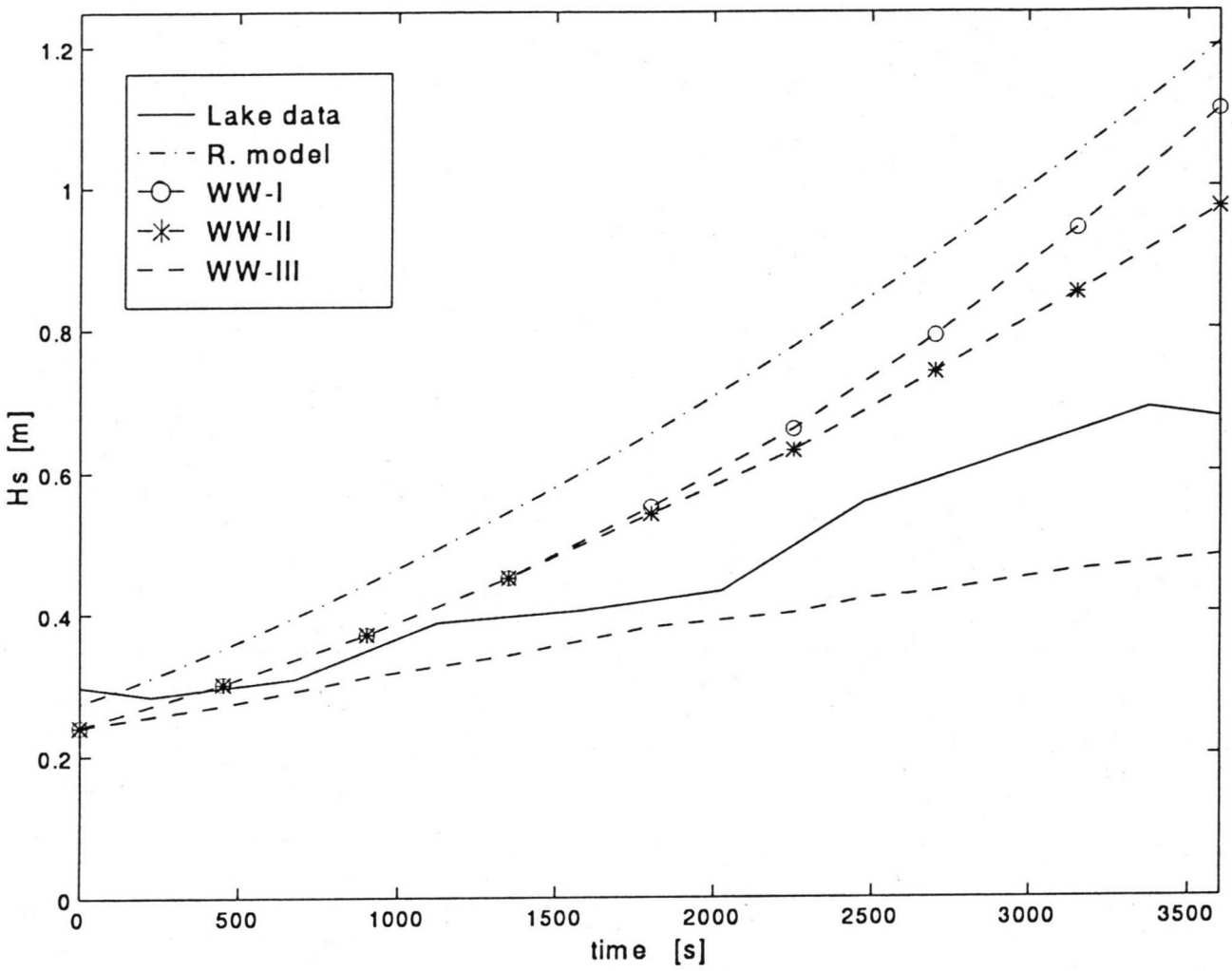

Figure 6.3 c Significant wave height Case III

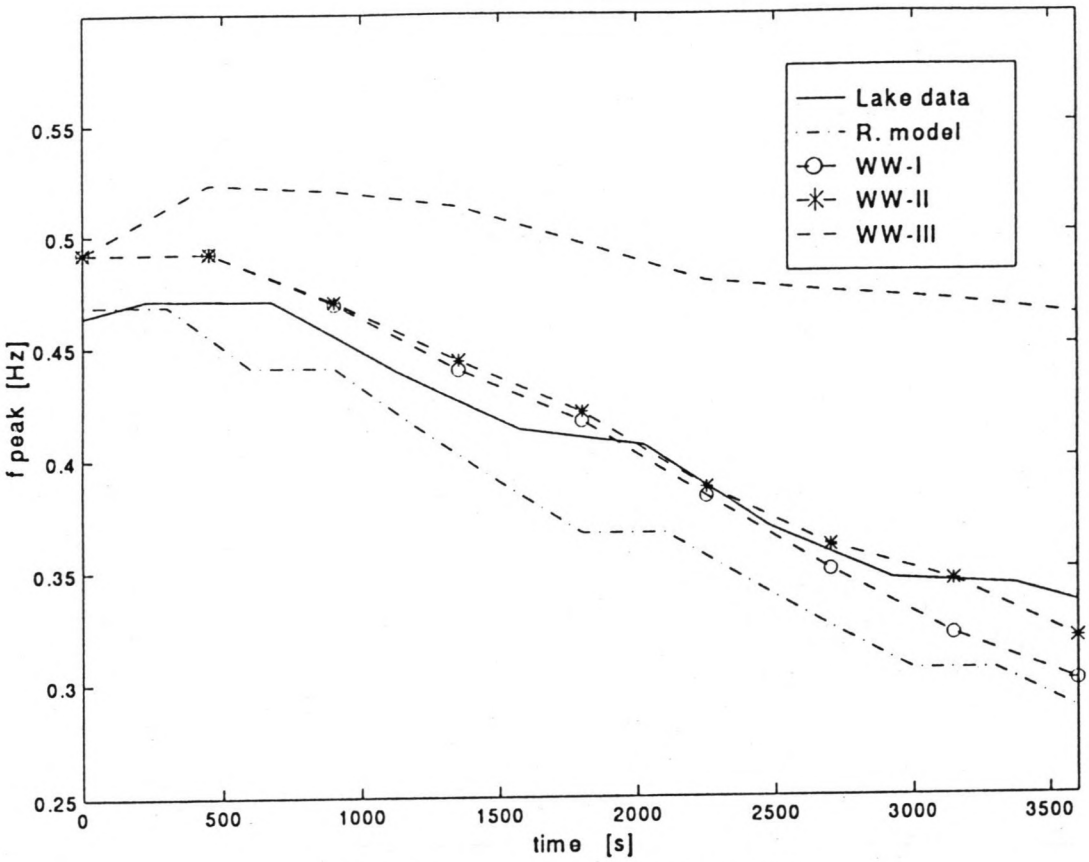

Figure 6.3 d Peak frequency Case III

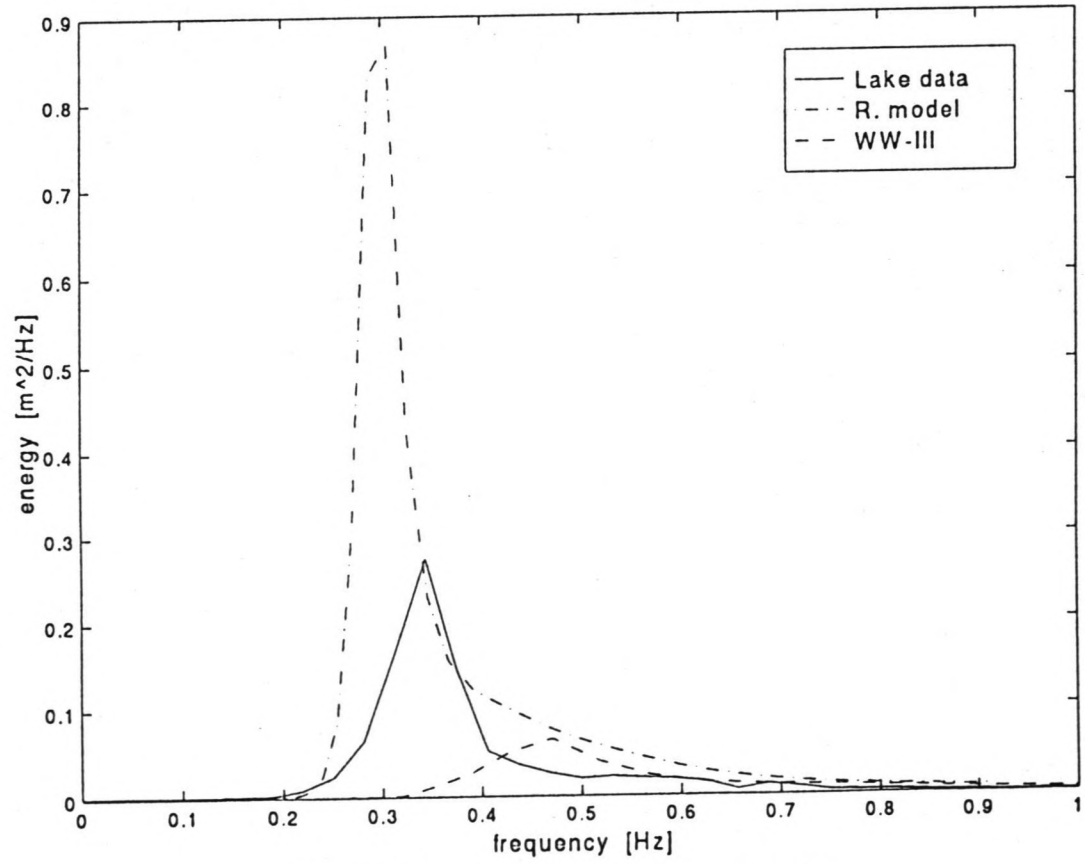

Figure 6.3 e Energy spectra at t_4 Case III

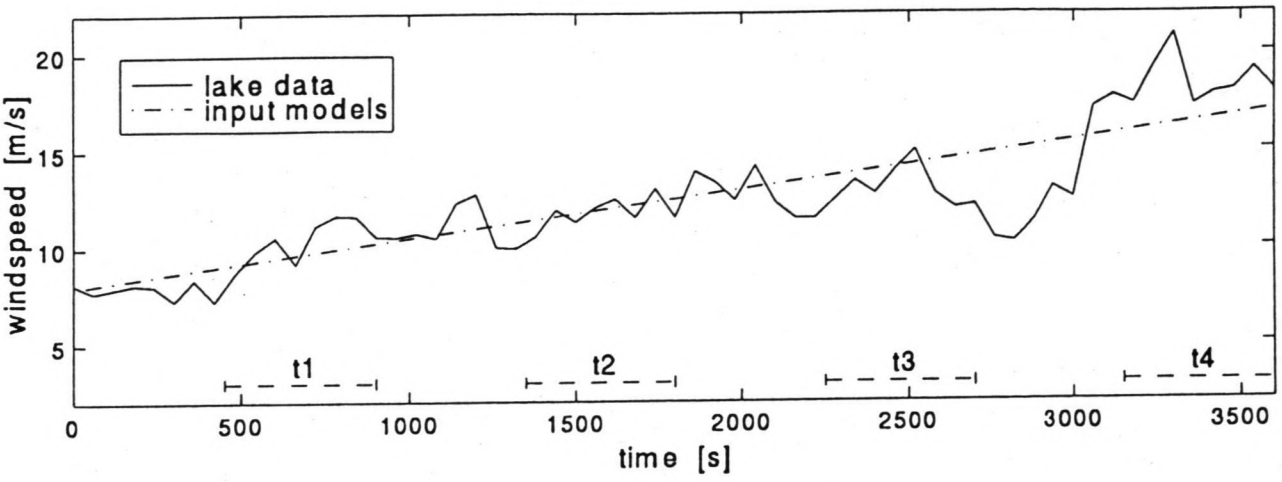

Figure 6.4 a Wind speed Case IV

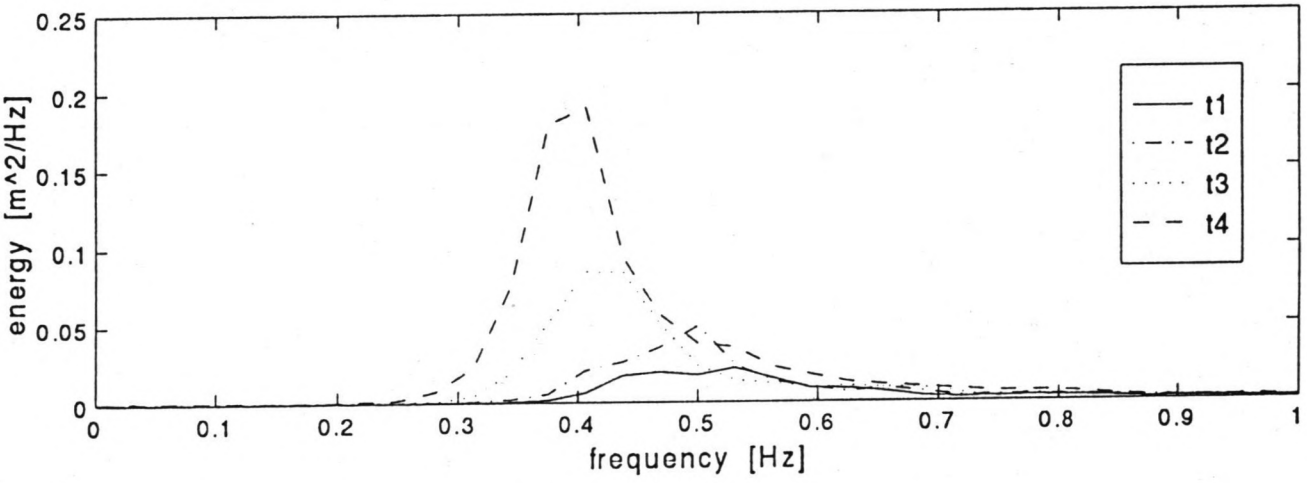

Figure 6.4 b Measured spectra Case IV

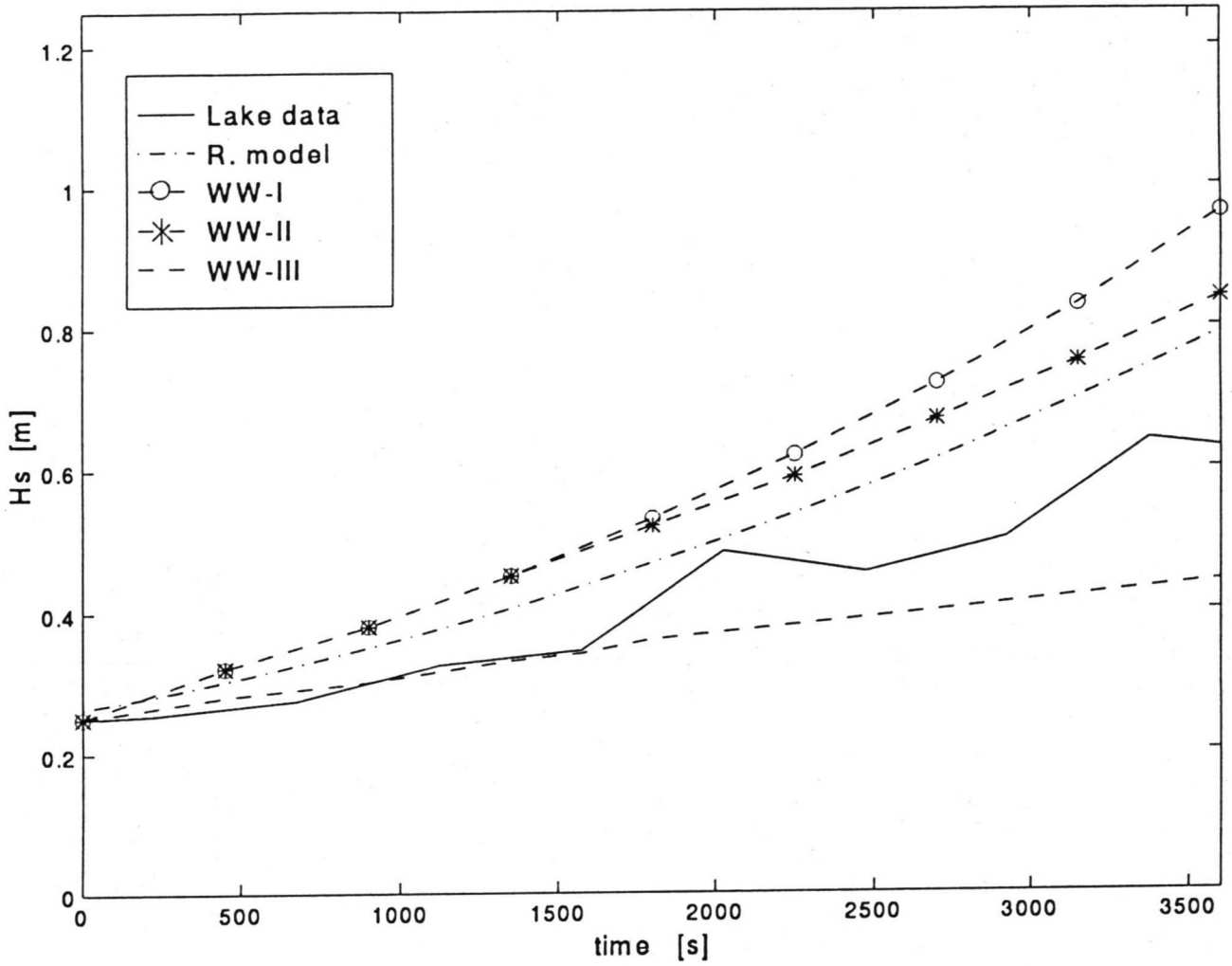

Figure 6.4 c Significant wave height Case IV

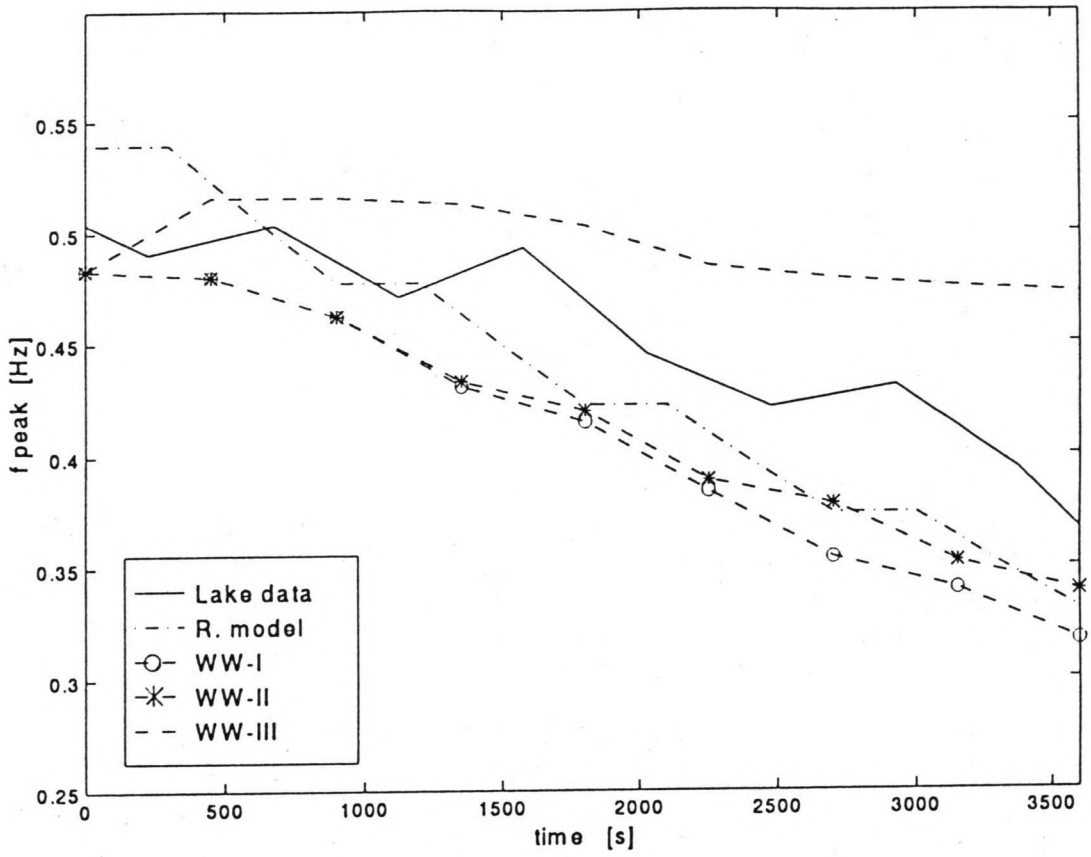

Figure 6.4 d Peak frequency Case IV

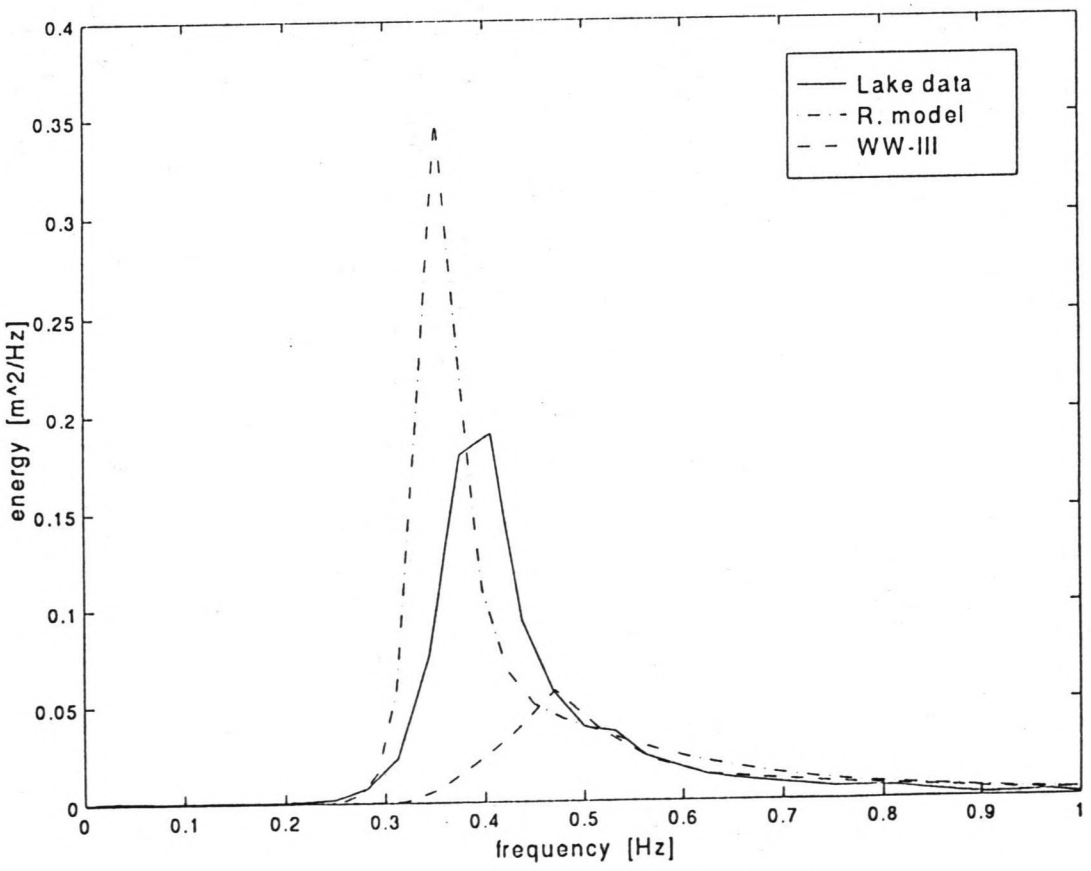

Figure 6.4 e Energy spectra at t_4 Case IV

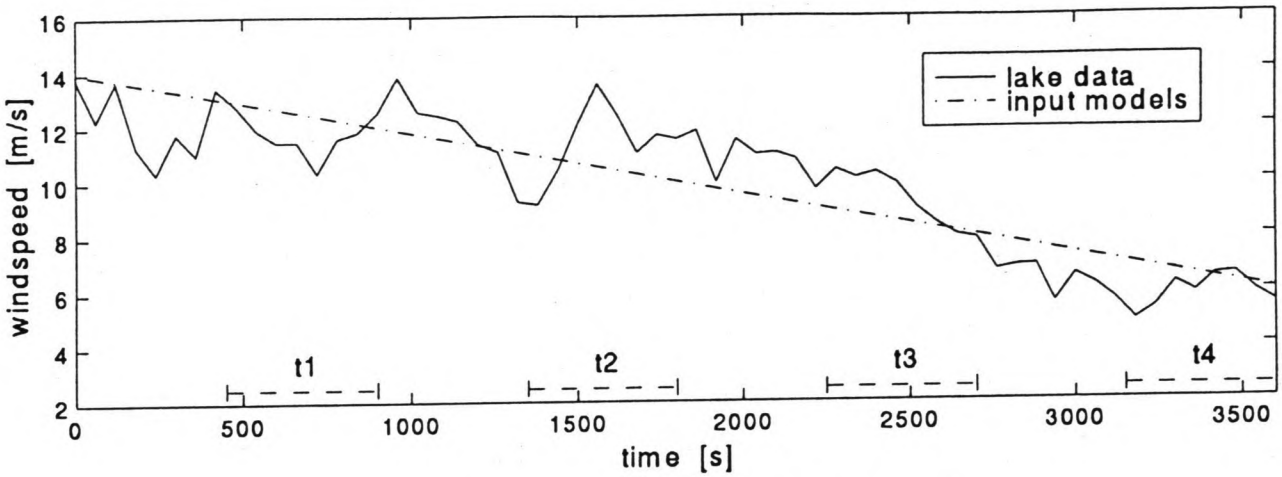

Figure 6.5 a Wind speed Case V

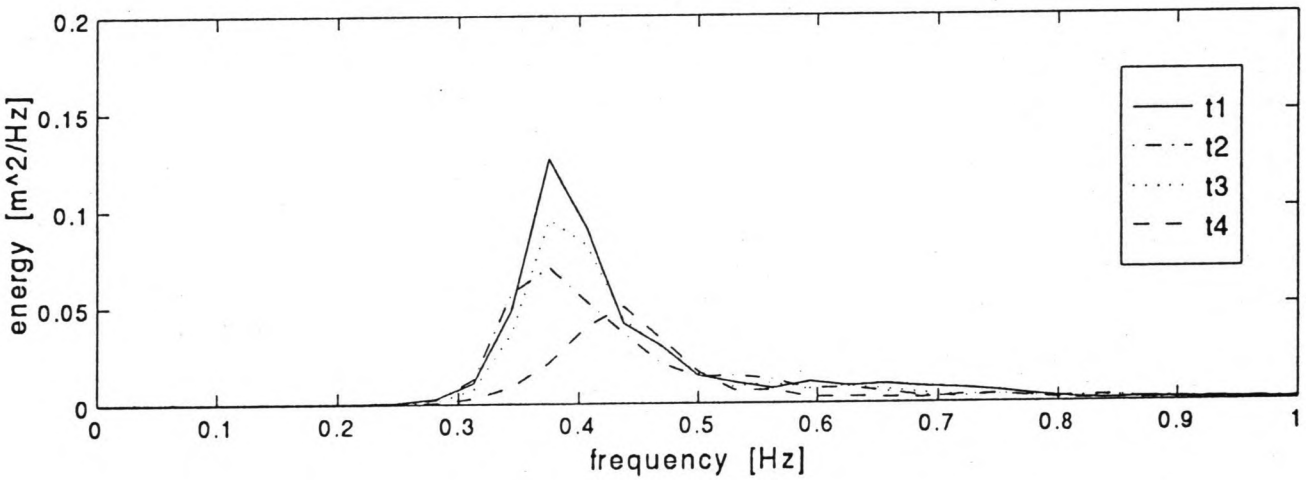

Figure 6.5 b Measured spectra Case V

Gradual decrease in wind speed

Case V is shown in figure 6.5 a,b,c,d,e. In this case the wind speed decreases gradually from 14 m/s to 6 m/s.

The wave height in Resio's model,WW-I and WW-II initially grows. Apparently the spectrum at the beginning is far from fully developed, so even a smaller wind speed can cause growth of the wave energy. However the lake data and WW-III show that a decreasing wind speed immediately causes energy loss. In WW-III the significant wave height is again too small.

Figure 6.5 c shows that for the lake data the peak frequency stays more or less constant for a while, finally increasing. On the other hand the peak frequency of WW-III responds very fast immediately.

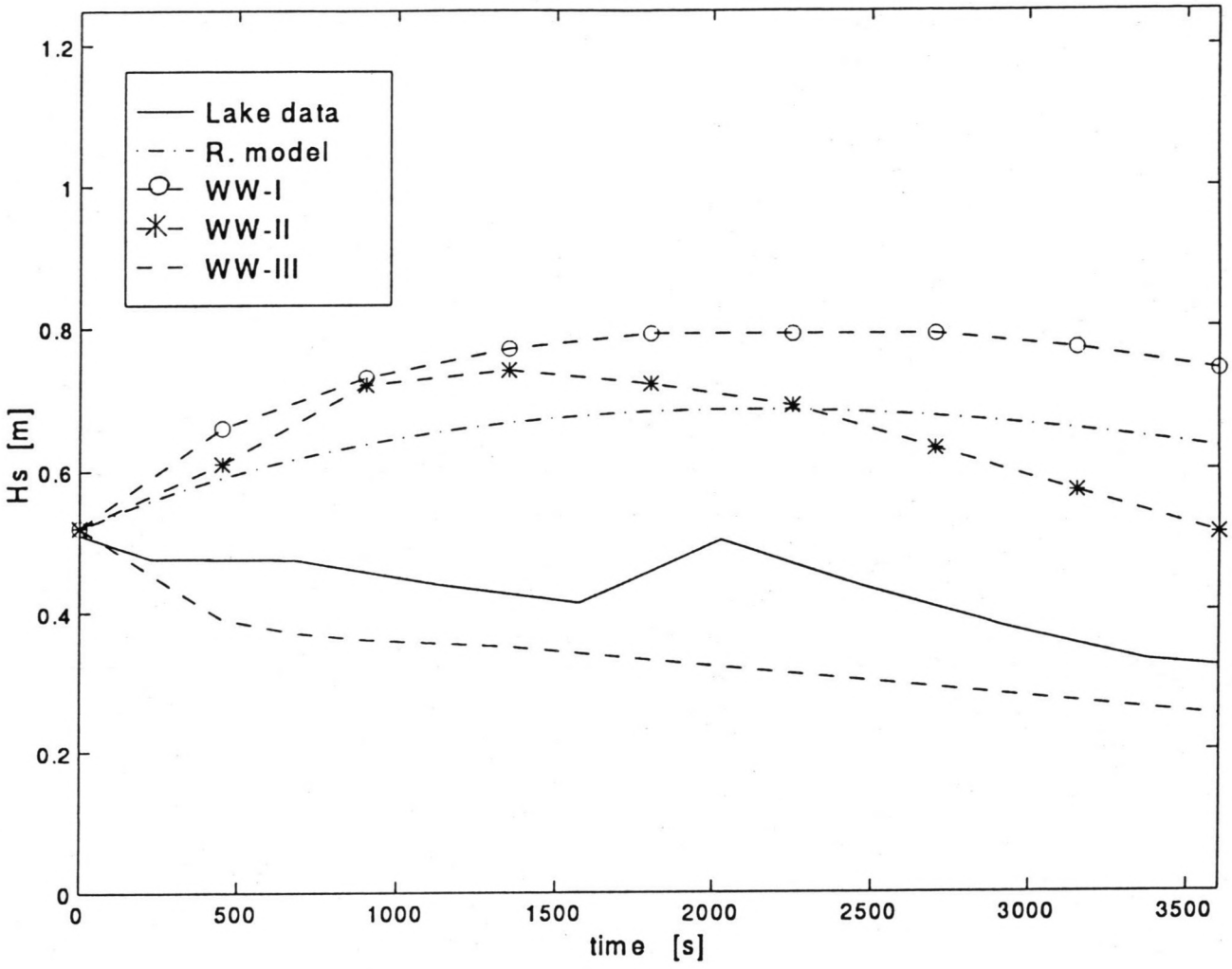

Figure 6.5 c Significant wave height Case V

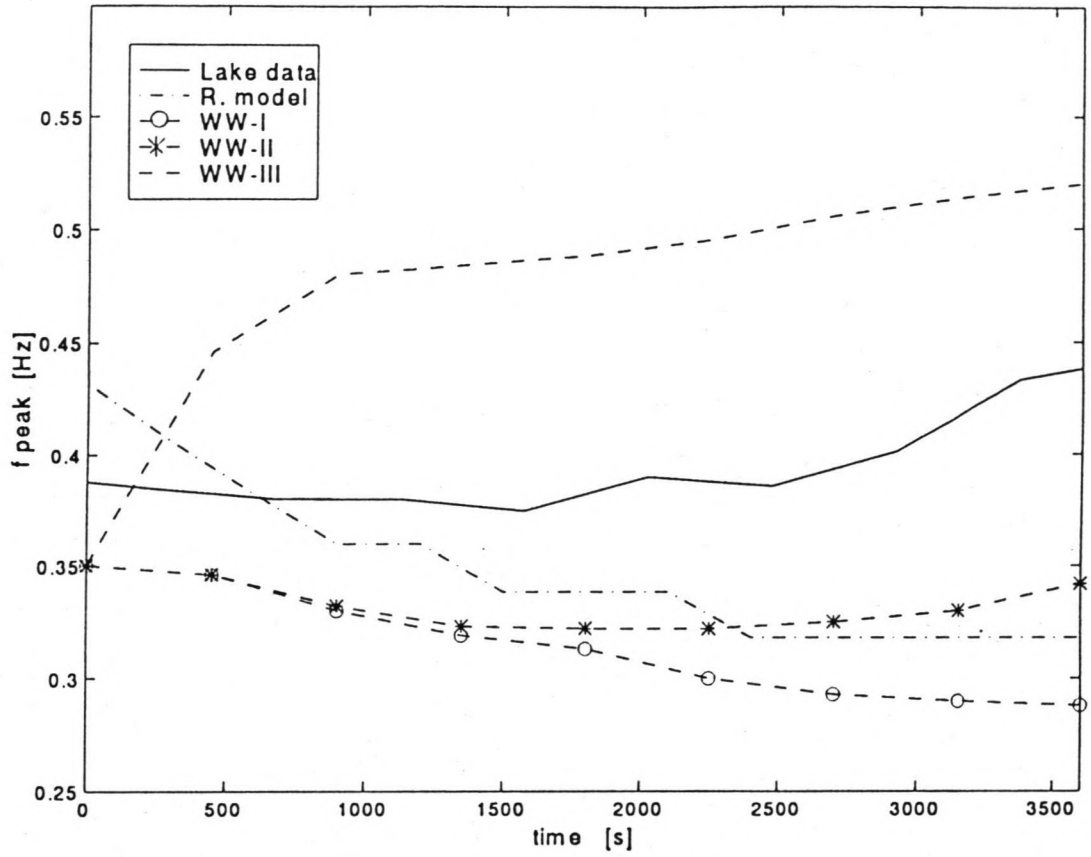

Figure 6.5 d Peak frequency Case V

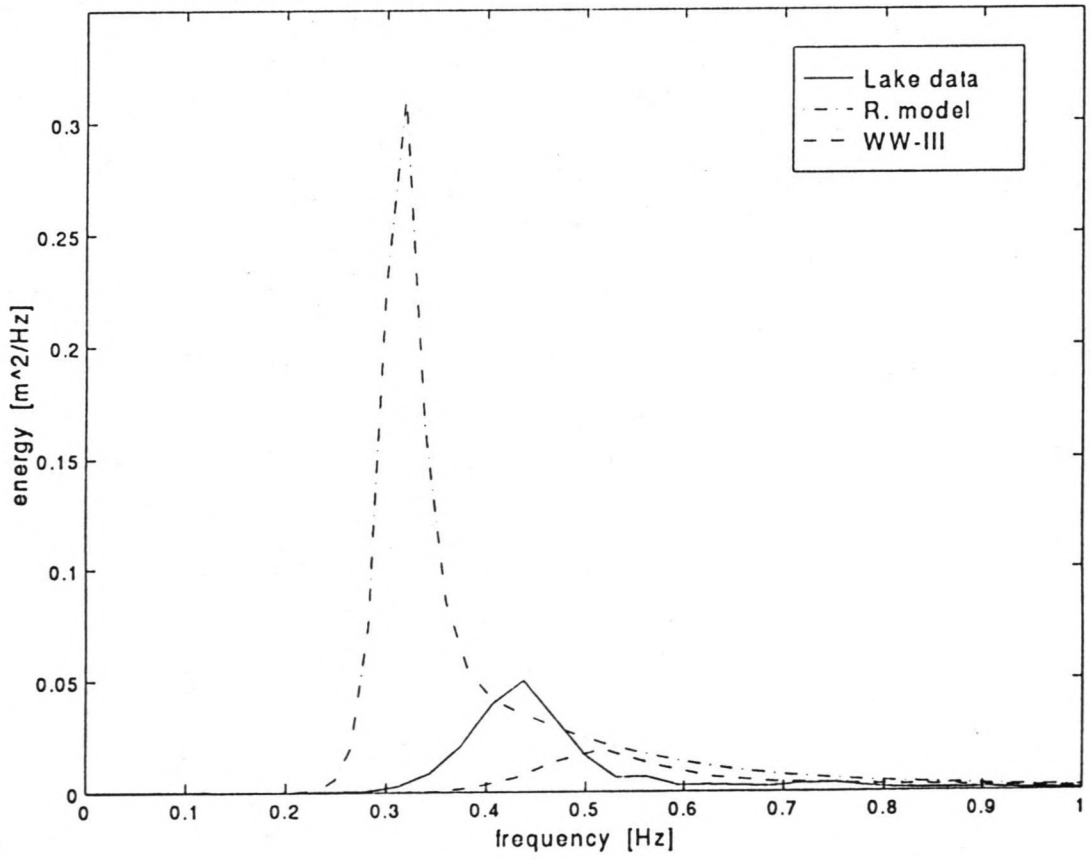

Figure 6.5 e Energy spectra at t_4 Case V

6.3 Discussion

Because both fetch and depth limitations play a role at the lake, the best results of the different model simulations should be expected from the WAVEWATCH calculations with the right lake dimensions (WW-III). However the results do not agree very well with the lake data, e.g. the significant wave heights are too small. The differences between the fetch-limited (WW-II) and unlimited (WW-I) calculations are small compared to difference with the WW-III calculations, so the limited depth of the lake has much more influence than the fetch. As the results of WW-I and WW-II give generally higher significant wave heights than Resio's model and the lake data, it is likely that the parameterization for bottom friction in WAVEWATCH gives too much dissipation of energy in the analysed situations. The 'standard' bottom roughness length scale (k_N = 0.04 m) was used, which seems to be too large.

Comparing the results of WW-I and Resio's model the differences are not negligible. The main difference of the two models is the way they calculate the nonlinear interactions, so the Discrete Interaction Approximation of WAVEWATCH seems to differ considerably from the full solution used in Resio's model, at least in these cases with changing wind speed. However, differences in numerical details can have a large influence, too.

It would be interesting to determine the factor a and $t_{½}$ of chapter 4 from the measurements. According to the numerical results $1/a$ and $t_{½}$ are in the order of magnitude of 100 s. However, for the calculation of the spectra record lengths of 7.5 minutes (450 s) were used. Because of the reliability of the results the record length cannot be taken much shorter. So the details of the spectral response, like a and $t_{½}$, were averaged out. In theory it could be possible to determine a and $t_{½}$ calculating the spectra e.g. every 10 s using record lengths of 7.5 minutes, so working with a large overlap. However, apart from the question whether this is really meaningful, the problem arises that the spectra are so irregular, that it is impossible to determine a or $t_{½}$. Because of the non-stationarity of the considered problem it might be better to replace the traditional data analysis by Fourier transforms by joint time-frequency analysis, e.g. wavelet-theory or Gabor Spectrogram (Doubrava, 1993).

Because of the difficulties of a detailed analysis of measurements, the only way to determine the time scale of the spectral response is with help of numerical models. The merit of the numerical results depends, of course, on the reliability of these models, which can be tested in terms of parameters like the significant wave height and peak frequency. If hindcasts of these parameters agree with the measurements, it could be assumed that the theoretically found values of a and $t_{½}$ are realistic. In case I and II, where the wind speed and significant wave heights are relatively small, Resio's model results agree reasonably with the lake data. To give a more solid confirmation of the model more suitable data should be analysed, especially for decreasing wind speed, or the model should be extended with possibilities for bottom friction and limited fetch. The discrepancies between WAVEWATCH and the measurements are so large that it is not meaningful to use this model to determine a and t numerically.

7. Conclusions and Recommendations

The numerical experiment with the model of Resio and Perrie demonstrates that the response of waves to a sudden change in wind speed is faster for high frequencies than for lower frequencies. The initial response is larger for increasing than for decreasing wind speed, but the time needed to reach a new equilibrium is of the same order of magnitude. The adjustment to a new equilibrium is faster for a larger increase in wind speed, but slower for a larger decrease.
The response of the spectrum to decreasing wind speed is dependent of the shape of the initial spectrum, as the relaxation of the spectrum to a lower wind speed is considerably slower for an initially more developed spectrum. For increasing wind speed the initial spectrum is less important.

Because of the averaging of the data by the Fourier transform and the irregularities of the spectra, it is not possible to determine the frequency-dependent time scales of the response from the measurements. Application of joint time-frequency analysis may give better information.

The comparison of the field measurements with the results of the model of Resio and Perrie and of WAVEWATCH show that the limited fetch of the lake has a small influence on the wave filed, but the influence of the bottom friction is considerable. So a comparison of the measurements with the results of the model of Resio and Perrie is only meaningful for short waves, which are not influenced by the limited depth of the lake. Reasonable results were found for two cases with suddenly increasing wind speed. For decreasing wind speed no suitable data was available.

It is not possible to give a good prediction of the wave field at Lake George with WAVEWATCH under changing wind conditions. The parameterization for the bottom friction seems to give too much energy dissipation. Tests in steady wind situations should be interesting.

References

Allender, J.H., J. Albrecht and G. Hamilton, 1983: Observations of directional relaxation of wind sea spectra. *J. Phys. Oceanogr.*, **13**, 1519-1525.

Bretschneider, C.L., 1958: Revisions in wave forecasting: deep and shallow water. *Proceedings of 6th Conference on Coastal Engineers, ASCE*, 30-67.

Coastal Engineering Research Center, 1984: Shore Protection Manual.

Donelan, M., M. Skafel, H. Graber,P. Liu, D. Schwab and S. Venkatesh, 1992: On the growth rate of wind-generated waves. *Atmosphere-Ocean*, **30(3)**, 457-478.

Doubrava, C., 1993: Nieuwe methoden voor signaalanalyse. *De Ingenieur*, **7-8**, 41-44.

Günther, H., W. Rosenthal and M. Dunckel, 1981: The response of surface gravity waves to changing wind direction. *J. Phys. Oceanogr.*, **10**, 718-728.

Groen, P. and R. Dorrestein, 1976: Zeegolven. *KNMI, Opstellen op oceanografisch en maritiem meteorologisch gebied*, **11**.

Hasselmann, D.E., M. Dunckel and J.A. Ewing, 1980: Directional wave spectra observed during JONSWAP 1973. *J. Phys. Oceanogr.*, **10**, 1264-1280.

Hasselmann, K., 1960: Grundgleichungen der Seegangsvoraussage, *Schiffstechnik*, **7**, 191-195.

Hasselmann, K., 1962: On the non-linear energy transfer in a gravity wave spectrum, Part 1. General theory. *J. Fluid Mech.*, **12**, 481-500.

Hasselmann, K., 1963: On the non-linear energy transfer in a gravity wave spectrum, Part 3. Evaluation of energy flux and swell-sea interaction for a Neumann spectrum. *J. Fluid Mech.*, **15**, 273-281.

Hasselmann, K., T.P. Barnett, E. Bouws, H. Carlson, D.E. Cartwright, K. Enke, J.A. Ewing, H. Gienapp, D.E. Hasselmann, P. Kruseman, A. Meerburg, P. Müller, D.J. Olbers, K. Richter, W. Sell and H. Walden, 1973: Measurements of wind-wave growth and swell decay during the Joint North Sea Wave Project (JONSWAP). *Dtsch. Hydrogh. Z. (Suppl.)* **A8**, 12.

Hasselmann, K., 1974: On the spectral dissipation of ocean waves due to white capping. *Bound. Layer Meteor.* **6**, 107-127.

Hasselmann, S. and K. Hasselmann, 1981: A symmetrical method of computing the nonlinear transfer in a gravity wave spectrum. *Hamburger Geophys. Einzelschriften*, **A52**.

Hasselmann, S. and K. Hasselmann, 1985: The wave model EXACT-NL. *Ocean wave modelling* (The SWAMP Group), 249-251, Plenum Press, New York and London.

Hasselmann, S., K. Hasselmann, J.H. Allender, T.P. Barnett, 1985: Computations and parameterizations of the nonlinear energy transfer in a gravity-wave spectrum. Part 2: Parameterizations of the nonlinear transfer for application in wave models. *J. Phys. Oceanogr.*, **15**, 1378-1391.

Holthuijsen, L.H., A.J. Kuik and E. Mosselman, 1987: The response of wave directions to changing wind directions. *J. Phys. Oceanogr.*, **17**, 845-853.

Komen, G.J., S. Hasselmann and K. Hasselmann, 1984: On the existence of a fully developed wind-sea spectrum. *J. Phys. Oceanogr.*, **14**, 1271-1285.

Madsen,O.S., Y.K. Poon and H.C. Graber, 1988: Spectral wave attenuation by bottom friction: theory. *Proc. 21th Int. Conf. on Coastal Eng.*, Malaga, ASCE, 492-504.

Miles, J.W., 1957: On the generation of surface waves by shear flows. Part 2. *J. Fluid Mech.*, **3**, 185-204.

Phillips, O.M., 1957: On the generation of waves by turbulent wind. *J. Fluid Mech.*, **2**, 417-445.

Phillips, O.M., 1958: The equilibrium range in the spectrum of wind-generated waves. *J. Fluid Mech.*, **4**, 426-434.

Phillips, O.M., 1960: On the dynamics of unsteady gravity waves of finite amplitude, Part 1. *J. Fluid Mech.*, **9**, 193-217.

Phillips, O.M., 1985: Spectral and statistical properties of the equilibrium range in wind generated gravity waves. *J. Fluid Mech.*, **156**, 505-531.

Quanduo, G. and G. Komen, 1993: Directional response of ocean waves to changing wind direction. *J.Phys. Oceanogr.*, **23**, 1561-1566.

Resio, D. and W. Perrie, 1991: A numerical study of nonlinear energy fluxes due to wave-wave interactions. Part 1: Methodology and basic results. *J. Fluid Mech.*, **223**, 609-629.

Snyder, R.L., F.W. Dobson, J.A. Elliott and R.B. Long, 1981: Array measurements of atmospheric pressure fluctuations above surface gravity waves. *J. Fluid Mech.*, **102**, 1-59.

SWAMP group, 1985: Ocean wave modelling, *Plenum Press*, New York and London.

Toba,Y., 1973: Local balance in the air-sea boundary processes, III. On the spectrum of wind waves. *J. Oceanogr. Soc. Japan*, **29**, 209-220.

Toba, Y., K. Okada and I.S.F. Jones, 1988: The response of wind-wave spectra to changing winds. Part I: Increasing Winds. *J. Phys. Oceanogr.*, **18**, 1231-1240.

Tolman,H.L.,1991: A third generation model for wind waves on slowly varying, unsteady and inhomogeneous depth and currents.*J.Phys.Oceanogr.*, **21**, 782-797.

Tracy, B.A. and D.T. Resio, 1982: Theory and calculation of the nonlinear energy transfer between sea waves in deep water, Report no. 11, *U.S. Army Engineer Waterways Experiment Station*, Vicksburg, U.S.A.

Vincent, C.L. and S.A. Hughes, 1985: Wind wave growth in shallow water. *J. Waterway, Port, Coastal and Ocean Engineering*, **111**, no.4.

Vledder, G.Ph. van, and L.H. Holthuijsen, 1993: The directional response of ocean waves to turning winds. *J. Phys. Oceanogr.*, **23**, 177-192.

WAMDI group, 1988: The WAM model - A third generation ocean wave prediction model. *J. Phys. Oceanogr.*, **18**, 1775-1810.

Webb, D.J., 1978: Non-linear transfers between sea waves. *Deep-Sea Res.*, **25**, 279-298.

Young, I.R., S. Hasselmann and K. Hasselmann, 1987: Computations of the response of a wave spectrum to a sudden change in wind direction. *J. Phys. Oceanogr.*, **17**, 1317-1338.

Young, I.R. and G.Ph. van Vledder, 1993: A review of the central role of nonlinear interactions in wind-wave evolution. *Phil. Trans. R. Soc. Lond.*, **342**, 505-524.

Zwarts, C.M.G., 1974: Transmission line wave height transducer. Proc. Int. Symp. on Ocean Wave Measurement and Analysis, 9-11 September 1974, New Orleans, La., No. 1, 605-620.

Acknowledgment

I thank Dr. Ian Young for the pleasant cooperation, comments and the availability of the measurement equipment on Lake George.
Thanks to Louis Verhagen I had a very good time in Canberra (without too many computer problems).

The trip to Australia was possible thanks to financial support of the University Fund Delft and the Dutch Royal Institute of Engineers.

List of symbols

a	parameter of growth rate
b	relaxation coefficient
A	linear growth term wind input
B	exponential growth term wind input
c	phase velocity
c_g	group velocity
C	proportionality factor of dissipation source function
d	water depth
D	interaction coefficient
E	energy density
f	frequency
f_p	peak frequency
f_w	friction factor
g	gravitational acceleration
G	coupling coefficient of nonlinear interactions
H_s	significant wave height
k	wavenumber
k_p	peak wavenumber
n	action density
S_{tot}	total source function
S_{in}	wind input source function
S_{ds}	dissipation source function
S_{nl}	nonlinear interactions source function
t	time
$t_{½}$	parameter of adjustment to new equilibrium
$u_{b,r}$	near-bottom orbital velocity
u_*	friction velocity at sea surface
U	wind speed
U_{10}	wind speed at 10 meters above water surface
$\hat{\alpha}$	mean wave steepness
$\hat{\alpha}_{pm}$	mean wave steepness of Pierson-Moskowitz spectrum
α_s	energy scale parameter of Toba's spectrum
ß	energy scale parameter of Phillips spectrum
δ	Dirac delta function
ϵ	total wave energy
θ	direction
θ_0	mean wave direction
θ_w	wind direction
ρ_a	density of air
ρ_w	density of water
τ	time scale of directional response
ω	radian frequency
$\bar{\omega}$	mean radian frequency

Appendix A Input parameters of the models

Model Resio and Perrie

* general

frequency increment factor 1.063
number of frequencies 43
number of points along locus 50
$\Delta\theta = 6.67°$

* Numerical experiment

frequency range $0.07 < f < 0.92$ Hz
time step $\Delta t = 5$ s

* Hindcasts

	frequency range [Hz]	time step [s]
Case I	0.20 - 2.59	0.5
Case II	0.15 - 1.95	1.0
Case III	0.07 - 0.92	5.0
Case IV	0.15 - 1.95	1.0
Case V	0.10 - 1.30	5.0

WAVEWATCH

geometric grid $\Delta x = 1$ km
$\Delta y = 1$ km

frequency increment factor 1.1
number of frequencies 25
$\Delta\theta = 15°$
$\Delta t = 45$ s

Case I and II $0.30 < f < 2.95$ Hz
Case III, IV and V $0.15 < f < 1.48$ Hz